NATIONAL ADVISORY COMMITTEE FOR AERONAUTICS

TECHNICAL NOTE

No. 1697

THE EFFECTS OF COMPRESSIBILITY ON THE LIFT, PRESSURE, AND LOAD CHARACTERISTICS OF A TAPERED WING OF NACA 66-SERIES AIRFOIL SECTIONS

By Morton Cooper and Peter F. Korycinski

Langley Aeronautical Laboratory
Langley Field, Va.

Washington

October 1948

NATIONAL ADVISORY COMMITTEE FOR AERONAUTICS

TECHNICAL NOTE NO. 1697

THE EFFECTS OF COMPRESSIBILITY ON THE LIFT, PRESSURE, AND LOAD CHARACTERISTICS OF A TAPERED WING OF NACA 66-SERIES AIRFOIL SECTIONS

By Morton Cooper and Peter F. Korycinski

SUMMARY

Tests of a 12-foot-span wing having 16-percent-thick NACA 66-series sections, 2:1 taper ratio, and an aspect ratio of 6 have been conducted in the Langley 16-foot high-speed tunnel at Mach numbers up to 0.69 to determine the effects of compressibility on the lift, pressure, and load characteristics of the wing.

The maximum lift coefficient increases from a value of 1.07 at a Mach number of 0.15 to a peak value of 1.135 at a Mach number of 0.25 and a Reynolds number of 3,500,000, then decreases, more rapidly at first, to a value of 0.895 at a Mach number of 0.50, after which it increases very rapidly to a value of 1.10 at a Mach number of 0.60 (limit of the maximum-lift tests). The increase in maximum lift coefficient at the higher Mach numbers is associated primarily with the unusually high acceleration of the flow around the sharp leading edge of the wing and with the rearward movement of the shock formation on the upper surface of the wing. At the lower Mach numbers serious losses in maximum lift coefficient were found to result from premature transition of the laminar boundary layer to a turbulent boundary layer caused by leading-edge roughness.

No significant changes in span load distribution and root bending-moment coefficients occurred throughout the Mach number range for all angles of attack below the stall. For all Mach numbers investigated, the spanwise distribution of normal loads on the wing can be predicted adequately for most structural purposes.

The formation of extensive local supersonic-flow regions over the upper surface of the wing, with peak local Mach numbers as high as 1.75, caused the center of pressure to move forward and thereby reduced the section twisting-moment and root twisting-moment coefficients.

INTRODUCTION

The significance of the interrelated influence of Reynolds number and Mach number in analyses of wind-tunnel maximum-lift data has been known for several years. During tests of a three-dimensional wing of NACA 0012 airfoil sections (reference 1) at low Mach numbers ($M < 0.37$), pronounced compressibility effects on the maximum lift coefficient were found in addition to the usual effects of Reynolds number on the maximum lift coefficient. These adverse compressibility effects, which occurred at relatively low speeds, were associated with the extremely high local induced velocities over the wing at high angles of attack and with the resultant inability of the flow to overcome the adverse pressure gradients. Similar effects were reported in a previous investigation (reference 2) of the maximum-lift characteristics of typical NACA 16-series propeller sections to obtain airfoil data applicable to the static-thrust condition. The results of reference 2 also showed an extremely rapid rise in maximum lift coefficient between Mach numbers of 0.48 and 0.60 for comparatively thick (15 percent) NACA 16-series sections. The necessity for an understanding of this rapid rise in maximum lift coefficient with an increase in Mach number is apparent from a consideration of the prediction of wing loads in high-speed maneuvers.

As a result of the scattered results from wind-tunnel tests (references 1 and 2) and flight tests (references 3 and 4) showing the significance of both Reynolds number and Mach number in determining the maximum-lift characteristics of airfoils, a comprehensive investigation of a series of conventional fighter-type wings was undertaken in the Langley 16-foot high-speed tunnel and the Langley 19-foot pressure tunnel. By means of tests in both tunnels, it was considered possible that the main effects of Mach number and Reynolds number on the maximum lift coefficient could be isolated and in that way individually evaluated. In addition, since the test wings were selected representative of fighter-type airplanes, important load and pressure data could be obtained as a corollary to the basic maximum-lift investigation. The data obtainable in the Langley 19-foot pressure tunnel at high Reynolds number and low Mach number would be useful for predicting landing loads and landing performance, and the data obtained in the Langley 16-foot high-speed tunnel at high Reynolds number and high Mach number would be applicable to high-speed maneuvers.

The first wing in the series to be investigated had a 12-foot span, NACA 230-series airfoil sections of varying thickness, a 2:1 taper ratio, and an aspect ratio of 6. The results of the high-speed investigation are presented in references 5 and 6, and the results of the low-speed investigation are presented in reference 7. The results of reference 5 indicate an increase in maximum lift coefficient to a peak value of 1.46 at a Mach number of 0.30 (Reynolds number of 4,500,000), then a rapid

decrease from a Mach number of 0.30 to 0.55, and a lower rate of decrease from a Mach number of 0.55 to 0.625. The magnitude of maximum lift at the low-speed peak and the Mach number at which it occurred depended on the Reynolds number; as the Reynolds number was increased, the maximum lift coefficient increased in magnitude and occurred at a lower Mach number (reference 7). It was also shown that the effect of Reynolds number on the maximum lift coefficient decreased appreciably after the low-speed peak maximum lift coefficient was reached.

The present paper contains the results of the high-speed maximum-lift tests conducted in the Langley 16-foot high-speed tunnel on a 12-foot-span wing having 16-percent-thick NACA 66-series sections, 2:1 taper ratio, and an aspect ratio of 6. In addition to the maximum-lift characteristics, high-speed bending-moment, twisting-moment, and pressure data representative of present-day fighter-type airplanes having wings of similar plan forms and sections are presented.

SYMBOLS

Free-stream conditions:

V_o	corrected airspeed, feet per second
a_o	speed of sound in air, feet per second
M_o	Mach number (V_o/a_o)
ρ_o	mass density of air, slugs per cubic foot
q_o	dynamic pressure, pounds per square foot $\left(\frac{1}{2}\rho_o V_o^2\right)$
p_o	static pressure, pounds per square foot
μ_o	coefficient of viscosity of air, slugs per foot-second
R_o	Reynolds number $(\rho_o \bar{c} V_o/\mu_o)$

Wing geometry:

S	wing area, square feet
b	wing span, feet
A	aspect ratio (b^2/S)
$\bar{c}$	mean chord, feet (S/b)
y	spanwise distance measured from plane of symmetry of wing, feet

x chordwise distance measured from airfoil leading edge, feet

c airfoil chord at any spanwise station, feet

α corrected angle of attack of wing at plane of symmetry, degrees

Force data:

L wing lift, pounds

C_L wing lift coefficient (L/q_oS)

Pressure data:

p local static pressure, pounds per square foot

P pressure coefficient $\left(\frac{p - p_o}{q_o}\right)$

P_{cr} pressure coefficient corresponding to a local Mach number of 1

c_n section normal-force coefficient $\left(\int_0^1 (P_L - P_U)\, d\left(\frac{x}{c}\right)\right)$

$\frac{c_n c}{\bar{c}}$ section normal-load parameter

C_N wing normal-force coefficient $\left(\int_0^1 \frac{c_n c}{\bar{c}}\, d\left(\frac{y}{b/2}\right)\right)$

C_{BM} root bending-moment coefficient

$$\left(\frac{1}{4}\int_0^1 \frac{c_n c}{\bar{c}}\,\frac{y}{b/2}\, d\left(\frac{y}{b/2}\right) = \frac{\text{Root bending moment}}{q_o S b}\right)$$

$c_{m_{x_1}}$ section pitching-moment coefficient due to normal forces about a line perpendicular to plane of symmetry and passing through 25-percent position of root chord

$$\left(\int_0^1 (P_L - P_U)\left(\frac{x_1}{c} - \frac{x}{c}\right) d\left(\frac{x}{c}\right)\right)$$

x_1 distance from leading edge of each spanwise station to line perpendicular to plane of symmetry and passing through 25-percent position of root chord, feet

$\frac{c_{m_{x_l}} c^2}{\bar{c}^2}$ section twisting-moment parameter

C_{TM} root twisting-moment coefficient about a line perpendicular to plane of symmetry and passing through 25-percent position of root chord

$$\left(\frac{1}{2} \int_0^1 \frac{c_{m_{x_l}} c^2}{\bar{c}^2} \, d\left(\frac{y}{b/2}\right) = \frac{\text{Root twisting moment}}{q_o S \bar{c}} \right)$$

Subscripts:

L	lower surface
U	upper surface
i	incompressible
c	compressible
cr	critical
max	maximum

MODEL, INSTALLATION, TESTS, AND CORRECTIONS

Model

Force and pressure tests were conducted in the Langley 16-foot high-speed tunnel with the test wing mounted on two conventional support struts as shown in figure 1. The test wing was constructed from solid steel to airfoil section ordinates given in table I. The geometric properties of the wing are as follows:

Span, feet	12
Wing area, square feet	24
Aspect ratio	6
Taper ratio	2:1
Wing sections	NACA 66 series (a = 0.6)
Thickness ratio	
Root section, percent	16
Tip section, percent	16
Design lift coefficient	
Root section	0.1
Tip section	0.2
Sweepback (along quarter-chord line), degrees	3.18
Dihedral (along quarter-chord line), degrees	0
Geometric twist (washout), degrees	1.55

The left semispan of the wing contained 210 pressure orifices, 35 orifices along the chord at each of six spanwise stations. (See fig. 2.) The locations of the spanwise stations at 10, 30, 50, 70, 85, and 95 percent of the wing semispan were selected to determine adequately the span load distribution and yet to minimize the local influence of the support struts on the nearby pressure orifices.

During all the tests the wing was frequently inspected and polished in order to maintain an aerodynamically smooth surface.

Installation

Force tests.- In order to obtain the basic lift data, the wing was mounted on two conventional support struts. (See fig. 1.) All pressure orifices were sealed within the wing, and a short fairing cap covered the pressure-tube exit located at the trailing edge of the root section of the wing (fig. 2). In addition to the conventional installation for the basic force tests, the wing was installed inverted with and without image struts and upright with image struts (fig. 3) to obtain the tare force and air-stream misalinement corrections as discussed in reference 8.

Pressure tests.- An auxiliary counterbalanced floating-tail strut was installed during tests to determine the pressure distributions over the wing. (See figs. 4(a) and 4(b).) The pressure tubes were brought out from the wing through a circular pipe section mounted rigidly to the wing and then through the floating-tail strut to multiple-tube manometers.

Tests

The basic force and pressure data were obtained for a range of angle of attack from -4° to the stalling angle for Mach numbers from 0.15 to 0.60. At Mach numbers from 0.60 to 0.69, the power limitations of the tunnel prevented the attainment of the higher angles of attack. The tests were conducted by varying the tunnel speed and maintaining a constant indicated angle of attack for the lower angle range (below 10° for the force tests and 6° for the pressure tests). For the higher angles, the data were obtained by holding a constant indicated tunnel Mach number and varying the angle of attack in small increments to define the stall sharply. Several additional tests were made to determine the influence of leading-edge roughness (covering approximately 5 percent of the chord measured along the surface) on the maximum lift coefficient.

The variation of average test Reynolds number with Mach number for the force and pressure tests is presented in figure 5. Individual curves are presented for the force and pressure tests because these

data were obtained 4 months apart and differences in the curves reflect changes in atmospheric conditions. A Reynolds number of 7.5×10^6 occurring at a Mach number of 0.7 (fig. 5) corresponds roughly to full-scale operation of present-day fighter airplanes at 40,000 feet altitude.

Corrections

Force tests.- The force data have been corrected for strut tares, air-stream misalinement, and wind-tunnel wall effects; these factors are discussed in reference 5. Specifically, the method of reference 8 was used to determine strut tares and air-stream misalinement corrections, and the methods of references 9, 10, and 11 were used to determine angle-of-attack and blockage corrections. The following table summarizes the magnitude of the corrections applied to the test data:

Correction	Maximum magnitude of correction	Maximum magnitude of correction at maximum lift
Air-stream misalinement angle, degrees $(\Delta\alpha_a)$	0.18	0.18
Angle-of-attack correction due to the jet-boundary-induced upwash at the lifting line, degrees $(\Delta\alpha_{l.l.})$	1.03	1.03
Angle-of-attack correction due to the jet-boundary-induced streamline curvature, degrees $(\Delta\alpha_{s.c.})$	.18	.18
Increment in lift coefficient due to struts (ΔC_{L_s})	.05	Negligible
Lift-coefficient increment due to strut seals $(-\Delta C_{L_{s.p.}})$	.025	.004
Lift-coefficient increment due to blockage, percent $\left(-\frac{\Delta C_L}{C_L} \times 100\right)$	1	1
Mach number increment due to to blockage, percent $\left(\frac{\Delta M}{M_o} \times 100\right)$	1/2	1/2

Pressure tests.- At the present time no adequate method is known for calculating the wind-tunnel wall effects on individual pressure readings obtained from static-pressure orifices on a relatively large wing at high speeds. In the analysis of the pressure data, attempts were therefore made to correlate the normal forces obtained from the integrated pressure measurements with the lift forces obtained from force measurements. This correlation showed that good agreement between the pressure and force data was obtained when the pressure data were based on a tunnel-empty calibration (force-test data are based on tunnel-empty calibration) and that recalibrating the tunnel to account for the local effects of the struts overcorrected the data by about $3\frac{1}{2}$ percent. All pressure data presented are therefore based on a tunnel-empty calibration.

All angle-of-attack corrections that were determined for the force-test data were applied to the pressure data.

PRESENTATION OF RESULTS

Force tests.- The data obtained in the force and pressure tests have been corrected to equivalent free-air conditions and are presented in standard nondimensional forms convenient for practical analysis. The lift-coefficient characteristics are summarized in the form of a lift "carpet" presented in figure 6. The abscissas shown on the lift carpet are angle of attack (for $M_o = 0.20$) and Mach number (for $\alpha = 0^\circ$). Lift curves for constant Mach numbers other than 0.20 are offset 4° in angle of attack for each 0.10 change in Mach number; lift curves for constant angles of attack other than 0° are offset 0.05 in Mach number for each 2° change in angle of attack. In several instances the data of the lift carpet have been replotted to illustrate pertinent lift characteristics and to afford comparisons with other available data. The data of figure 7(a), taken from figure 6, permit a comparison of the experimental and theoretical variation of lift coefficient with Mach number for angles of attack from -4° to 12° and show the influence of the critical Mach number in affecting this comparison. The variation of the lift coefficient with Mach number at angles of attack near the stall is shown in figure 7(b); the maximum-lift-coefficient curve is included to show the limiting conditions of lift. The critical Mach number curve has again been added to define subcritical and supercritical flow regions. The critical Mach number used in this paper is that free-stream Mach number at which the speed of sound is first reached locally on the airfoil for a given configuration. Figure 8 shows the variation of the maximum lift coefficient with Mach number and the effect of leading-edge roughness on the maximum lift coefficient at low speeds. Flight-test data of reference 12 have been added to figure 8 to permit a comparison of the tunnel results with flight data obtained for a similar wing.

Pressure tests.- Representative pressure distributions obtained at the mid-semispan station are shown in figure 9 for constant angles of attack and variable Mach numbers and in figure 10 for constant Mach numbers and variable angles of attack. Contours of constant pressure along the entire span of the wing are presented for Mach numbers of 0.20, 0.40, and 0.60 in figures 11 to 13. A comprehensive compilation of the pressure distributions for all six spanwise stations is presented in reference 13. In order to provide a comparison of the maximum-lift characteristics of the NACA 230-series wing reported in reference 5 with those of the NACA 66-series wing presented herein, representative pressure distributions of the two wings are plotted in figure 14. The pressure distributions for the 230-series wing were taken at the 47-percent semispan station. The chordwise pressure distributions obtained from measurements over the left semispan of the wing were integrated to yield the section normal-force coefficient c_n and section pitching-moment coefficient $c_{m_{x_l}}$.

The spanwise distribution of the section normal-force coefficient is presented in figure 15 in the form of span load distributions for representative wing normal-force coefficients for Mach numbers of 0.20, 0.40, and 0.60. Figure 15(a) also contains calculated span load distributions obtained by the method of reference 14 for a Mach number of 0.20. The wing normal-force coefficients obtained by the integration of the span load distributions are presented in figure 16 as a normal-force carpet. The method of presentation of the normal-force data is the same as that used for presenting the lift data. The variation of the root bending-moment coefficient with Mach number, obtained from the moment of the span load distributions about the plane of symmetry, is shown in figure 17 along with the values of root bending-moment coefficients obtained by integration of the theoretical span load distributions for a Mach number of 0.20. The section pitching-moment data along the span have been presented in figure 18 for representative normal-force coefficients for Mach numbers of 0.20, 0.40, and 0.60. These data have been presented in the form of a twisting-moment parameter $c_{m_{x_l}}\left(\frac{c}{\bar{c}}\right)^2$ which is referenced to a line perpendicular to the plane of symmetry and passing through the 25-percent position of the root chord. The integration of these twisting-moment distributions yields the wing twisting-moment coefficients about the 25-percent position of the root chord, and these integrated coefficients are plotted against angle of attack in figure 19.

DISCUSSION

Lift and Normal-Force Characteristics

Lift carpet.- The general lift and stalling characteristics of the test wing, as well as certain lift-curve characteristics which may be

associated with 66-series airfoils, are readily discernible in the lift carpet presented in figure 6. Beyond the limit of the low drag range, which is reached at an angle of attack of approximately $5\frac{1}{2}^\circ$, the lift curve shifts and a decrease in slope occurs. This phenomenon, which is characteristic of the airfoil section, is discussed in reference 15 and has been previously reported for a tapered wing in reference 16. At Mach numbers above 0.50, the shift or jog in the lift curves tends to disappear. The elimination of this jog is associated with the increased Reynolds numbers which occur at the higher Mach numbers, and, as a result, the extent of the laminar separation near the leading edge is reduced. The lift curve for a Mach number of 0.55 has a decreasing slope which starts at an angle of attack of about 4° and persists up to 10°; at angles of attack beyond 10°, the slope of the lift curve increases rapidly to approximately 5.7 per radian, a value considerably larger than the lift-curve slope of 4.8 per radian determined for the low angle-of-attack range. Lift curves for Mach numbers above 0.55 follow a similar but more pronounced pattern. As will be discussed in a following section, this initial reduction in lift-curve slope and the subsequent rapid rise are associated with the build-up of trailing-edge separation and the formation of extensive regions of supersonic flow on the forward portion of the upper surface of the wing.

Comparison of lift and normal-force data.- In general, the lift and normal-force data (figs. 6 and 16) obtained independently during these tests show very good agreement, and any qualitative discussion of either the lift or the normal-force characteristics is directly applicable to the other. In particular, however, a comparison of figures 6 and 16 does show a marked difference in the vicinity of the stall at low Mach numbers. Part of this discrepancy in maximum lift coefficient can be attributed to a difference in the Reynolds number (fig. 5) between the force and pressure tests. In addition, a varying type of stall at low Mach numbers was also encountered during several repeat force tests at a given Mach number (approximately a given Reynolds number) and is associated with the extremely sensitive reaction of this type of airfoil to "apparent" flow changes caused by a variation in surface conditions. Although attempts were made to maintain an aerodynamically smooth surface at all times, the results at low Mach numbers near the stall were probably influenced by surface conditions. This phenomenon will, however, be of no practical importance because of its occurrence at low Reynolds numbers only. A typical present-day fighter airplane will have a landing Reynolds number of about 6,000,000, a value which is above this extremely critical Reynolds number range. (A similar phenomenon was encountered in a preliminary investigation prior to the main tests reported in reference 17.)

Variation of lift coefficient with Mach number.- The experimental rise in lift coefficient with Mach number shown in figure 7 is compared with theoretical predictions based on the Glauert-Prandtl theory modified for a finite span by the method of reference 18. If the

two-dimensional lift-curve slope is assumed to be 2π, the theoretical rise in lift coefficient due to compressibility is given by:

$$\frac{C_{L_c}}{C_{L_i}} = \frac{A + 2}{2 + A\sqrt{1 - M_o^2}}$$

The data of figure 7 show excellent agreement between the experimental and theoretical variations for all subcritical Mach numbers up to an angle of attack of 12°. As might be expected from the force data, the pressure distributions for a representative angle of attack $\alpha = 6.75°$ (fig. 9(a)) show no unusual or radical Mach number effects. At supercritical Mach numbers, however, there is a marked disagreement between the experimental and theoretical curves; a disagreement which increases in magnitude as the angle of attack is increased and which, because of its magnitude, invalidates the use of this extrapolation to predict even roughly the lift coefficient in supercritical flows. At angles of attack greater than 12° (fig. 7(b)), the approximations inherent in this linearized theory are sufficiently in error to underestimate appreciably the magnitude of the lift coefficient in subcritical flow and hence prohibit its use.

In the supercritical region, the variation of the lift coefficient with Mach number for moderate and high angles of attack is associated with the build-up of trailing-edge separation and the formation of shock on the upper surface of the wing. The decrease in lift coefficient which occurs when the critical pressure is exceeded reaches a minimum in the Mach number range of 0.50 to 0.60 (fig. 7(b)); for a representative angle of attack of 11.1° the minimum occurs at a Mach number of 0.55, while for $\alpha = 13.2°$, it occurs at a Mach number of 0.50. An examination of the pressure diagrams (figs. 9(b) and 9(c)) at the corresponding minimum points ($M_o = 0.55$ at $\alpha = 11.1°$ and $M_o = 0.50$ at $\alpha = 13.2°$), immediately shows that the amount of separation and the loss in lift over the rear portion of the upper surface resulting from this separation is a maximum at these points and, furthermore, the positive contribution of the under surface to the lift is a minimum at these points. After the minimum value of the lift coefficient in the supercritical region is reached, a further increase in Mach number will result in a very rapid increase in the lift coefficient. At a Mach number of 0.55 and an angle of attack of 13.2° (fig. 9(c)), a well-established shock is evident with a local supersonic region of about 14 percent of the chord and a peak local Mach number of about 1.75. A further increase in Mach number to 0.60 moves the shock rearward and extends the local supersonic region to about $27\frac{1}{2}$ percent of the chord. The increment of lift coefficient caused by the local supersonic flow is immediately apparent from a consideration of the increased areas under

the pressure-distribution curves. According to the data of figure 6 it is probable that no further significant increase in lift coefficient would occur with increasing Mach number for 13.2° angle of attack. The data of figure 6 show that the angle of attack for maximum lift is 13.5° for a Mach number of 0.60 and that the angle for maximum lift decreased with increasing Mach number. Hence, since 13.2° will be the angle for maximum lift for some Mach number only slightly in excess of 0.60, the distribution presented for a Mach number of 0.60 is assumed to be sufficiently close to the maximum pressure distribution for all practical purposes.

For an angle of attack of 11.1°, an extensive supersonic region of $22\frac{1}{2}$ percent of the chord is formed when the free-stream Mach number is raised from 0.55 to 0.60. This broadening of the local supersonic region results, as in the case of $\alpha = 13.2°$, in a rapid rise in lift coefficient. Surprisingly enough, a slight reduction in separation occurs with this increase in Mach number.

For an angle of attack of 14°, the data of figure 7(b) show a rapid loss in lift coefficient at Mach numbers exceeding 0.575. The indications are, therefore, that after the maximum lift coefficient is reached (for a given angle of attack) with a strong shock present in the flow, a further increase in Mach number will result in a serious loss of lift.

Maximum lift coefficient.- The value of the maximum lift coefficient (fig. 8) increased from a value of 1.07 at a Mach number of 0.15 to a peak value of 1.135 at a Mach number of approximately 0.25 (a Reynolds number of 3,500,000). This increase of maximum lift coefficient was essentially a Reynolds number effect. Beyond a Mach number of 0.25, the increase in maximum lift coefficient with Reynolds number was counteracted by adverse compressibility effects resulting in a flow breakdown characterized by laminar separation from the leading edge of the wing and a decrease in maximum lift coefficient. The value of the maximum lift coefficient continued to decrease until the minimum attainable critical Mach number of approximately 0.33 was reached during the pressure tests. (Because of the varying type of stall at low Mach numbers and the difference in Reynolds number between the force and pressure tests, it is quite possible that the minimum attainable critical Mach number was slightly lower during the force tests.) As the Mach number was further increased, the forward pressure peaks broadened and decreased in magnitude; these changes thereby tended partly to compensate for the continued loss in maximum lift and to reduce the rate of decrease of maximum lift with Mach number between Mach numbers of 0.35 and 0.50. After the minimum value of the maximum lift coefficient (0.895) was attained at a Mach number of 0.50, further increases in Mach number resulted in rapid increases in maximum lift coefficient to a value of 1.10 at a Mach number of 0.60 (the limit of the tests).

Flight tests reported in reference 12 for an airplane having a wing whose plan form and airfoil sections are very similar to the model wing produced data which are in very close agreement with the present data. (See fig. 8.) The flight data were obtained at an altitude of 32,300 feet under conditions whereby the flight Reynolds number was roughly equal to the test Reynolds number. The minimum value of the maximum lift coefficient for both tests (fig. 8) was approximately 0.9 and occurred at a Mach number of about 0.50. In each case this minimum was followed by a rapid rise in maximum lift coefficient which reached a secondary peak value of 1.095 in the flight tests. Although no secondary peak had been reached in the tunnel tests, a comparison of the tunnel tests with the flight tests shows that the final maximum lift coefficient of 1.1 obtained at a Mach number of 0.60 would be very close to the value obtained at the secondary peak of the test wing.

These maximum-lift characteristics of the 66-series wing are considerably different from those of the 230-series wing discussed in reference 5. Unlike the 66-series wing the value of the maximum lift coefficient for the 230-series wing decreased with Mach number throughout the range of the tests after attaining its peak value at a Mach number of about 0.30. This marked difference in maximum-lift characteristics of the wings is of extreme importance from structural-design considerations in addition to aerodynamic aspects. The representative pressure distributions (fig. 14) for both wings show that the build-up and rearward movement of the shock formation, though much more pronounced for the 66-series wing, is somewhat similar for both configurations. The most significant difference in the pressure distributions is the location of the peak points. From figure 14 the pressure peaks for the 66-series wing are seen to occur within about 1 percent of the chord after a very rapid acceleration around the leading edge. Furthermore, these peak locations do not vary significantly over the Mach number range. Consequently, as the shock moves downstream along the chord, the highly negative pressures extend over larger portions of the chord, and the lift coefficient is thereby appreciably increased. In contrast to these results, the pressure distributions of the 230-series wing (fig. 14) show less rapid accelerations around the leading edge and a peak pressure that moves downstream as the Mach number is increased. This loss in lift in the vicinity of the leading edge of the 230-series wing overcompensates for the gain caused by the rearward shock movement and results in a net decrease in the maximum lift coefficient.

As to the fundamental explanation of the high accelerations around the leading edge of the 66-series wing, inadequate experimental data exist from which any positive conclusions can be drawn. It is quite probable, however, that because of the sharpness of the leading edge of the airfoil a very small, localized separation region is formed on the upper surface in the vicinity of the leading edge (reference 19). In case of such a phenomenon, the main flow would then turn supersonically around this region and become reattached to the airfoil surface. The flow would then be expanded more than is required by the physical

boundary and would thus be directed back to the airfoil surface. This overexpansion would result in the abnormally high pressure peaks very close to the leading edge. The flow then undergoes a slight stabilizing compression prior to the main deceleration shock. The probability of an overexpansion at the leading edge is also indicated by the fact that the 66-series wing attained peak local Mach numbers as high as 1.75 as compared to 1.55 for the 230-series wing.

It is, therefore, apparent that the main difference in maximum-lift characteristics at the higher Mach numbers is essentially a leading-edge effect and that airfoils having sharp leading edges such as the NACA 66 series will exhibit the rise in maximum lift coefficient with Mach number, whereas airfoils having blunter leading edges such as the NACA 230 series will not exhibit this rise.

Leading-edge-roughness tests were made at low Mach numbers to determine the effect of the boundary layer upon the maximum lift coefficient. The data of figure 8 show that the condition of the leading edge is of utmost importance in determining the maximum lift coefficient and that serious losses in maximum lift will result from premature thickening and transition of the boundary layer in the vicinity of the leading edge. No significant Mach number or Reynolds number effect occurred within the Mach number or Reynolds number range of the roughness tests, and thus the presence of a fully developed turbulent boundary layer without excessive pressure peaks was indicated.

Stalling characteristics.- An examination of the force data of figure 6 shows that a discussion of the general stalling characteristics can be divided into three representative groups: low-speed stall ($M_o = 0.20$), moderate-speed stall ($M_o = 0.40$), and high-speed stall ($M_o = 0.60$). In order to trace the build-up and spanwise progression of the stall, pressure contours for various high angles of attack for Mach numbers of 0.20, 0.40, and 0.60 have been presented (figs. 11 to 13) in addition to the pressure distributions for the mid-semispan station. (See fig. 10.)

The low-speed stall (figs. 10(a) and 11) is essentially characterized by a laminar separation of the flow from the leading edge with a sharply defined stall and a rapid flow breakdown. The pressure distributions for various increasing angles of attack (fig. 10(a)) show the progressively increasing leading-edge peak and only slight increases in trailing-edge separation. At an angle of attack of 17.5°, the adverse pressure gradient was of sufficient strength to cause a sharp flow breakdown at the leading edge (evidenced by two distributions, one stalled and one unstalled, at $\alpha = 17.5°$). Although the stall rapidly covered the entire wing, the first station observed to stall was located at $\frac{y}{b/2} = 0.1$ (fig. 11(e)), and then the stall progressed almost instantaneously to the mid-semispan (fig. 11(f)). Although the stall finally reached the tip, the intensity was not very severe from $\frac{y}{b/2} = 0.8$ outboard for this Mach number (0.20) and all other Mach numbers tested.

The character of the stall at a Mach number of 0.40 (figs. 10(b) and 12) was entirely different from that at a Mach number of 0.20 (figs. 10(a) and 11). The maximum lift coefficient was attained at an angle of attack of 13.6°, the lift curve having a rounded peak and only a small variation in lift on either side of the peak (fig. 6). Stall in this case was caused by a build-up of trailing-edge separation which gradually extended forward (figs. 10(b) and 12). Stall began first at the mid-semispan station and spread slowly to cover the rest of the wing (fig. 12). The pressure distribution for an angle of attack of 17.2° (fig. 10(b)), 3.6° beyond the maximum lift, though showing pronounced separation, does not indicate a serious loss in lift.

The high-speed stall (M_o = 0.60) occurred sharply after a slight rounding off of the lift curve (fig. 6). Increasing the angle of attack from 10.0° to 12.8° (fig. 10(c)) resulted in a large increase in the local supersonic region and, therefore, in a large increase in lift-curve slope. As the angle of attack was further increased to the stall, the amount of separation increased and resulted in the rounding off of the lift curve. The stall was probably precipitated by trailing-edge separation accompanied by a large loss in lift when the shock reached sufficient strength to cause a complete flow breakdown. The gradual recompression shown in figure 10(c) for an angle of attack of 13.5° is believed to be caused by the shock moving a significant distance above the airfoil over a region of separated flow. In this way, the pressure discontinuity which may exist in the free stream will be recorded by the surface orifices as a gradual compression through the separated flow. The spanwise contours of figure 13 show that stall occurred first at $\frac{y}{b/2} = 0.5$ and progressed inboard and outboard.

Load Distributions

Span load distributions.- The span load distributions for representative normal-force coefficients for Mach numbers of 0.20, 0.40, and 0.60 (fig. 15) show no significant shift in load or center of pressure with Mach number even when strong shock formations are present on the wing. A comparison of the experimental data with theoretical calculations based on the method of reference 14 is made at a Mach number of 0.20. The good agreement for all normal-force coefficients below the stall indicates that the spanwise distribution of normal loads can be predicted adequately for most structural purposes.

Root bending-moment coefficients.- The variation of the root bending-moment coefficient with Mach number for various representative normal-force coefficients (fig. 17) shows no compressibility effects and, for all practical purposes, may be considered constant. The peak values of the bending-moment coefficient vary considerably with Mach number and in general reflect the variation of maximum lift coefficient with Mach number. Bending-moment coefficients obtained from the

theoretical span load distributions show, as would be expected, very good agreement with the experimentally determined coefficients.

Twisting-moment distributions.- The root twisting-moment distributions presented in figure 19, in general, show the influence of stall and shock formation on the wing. Figure 18(a) ($M_o = 0.20$) shows the progressive build-up of negative twisting load at the tip with increasing normal-force coefficient. The fact that the tip twisting-moment parameter is larger than the root parameter indicates that the longer tip-moment arm from the reference axis to the section center of pressure has a greater influence on the local twisting-moment parameter than the larger root chord. The sudden increase in twisting moment at the root at a normal-force coefficient of 1.00 is attributed to the stall initially occurring at $\frac{y}{b/2} = 0.1$ and to the accompanying rearward movement of the center of pressure at this station. The essentially flat distribution for a normal-force coefficient of 0.72 was obtained after the wing stall became extensive.

Figure 18(b) presents the twisting-moment parameter for a Mach number of 0.40 and, as in the case of a Mach number of 0.20, closely follows the stall pattern. An irregular increase in the twisting-moment parameter for a normal-force coefficient of 0.95 occurring at the wing mid-semispan is again attributable to stall. The severity of the stall increases with increasing angle of attack and can be seen to spread out from the middle of the semispan.

For the high-speed condition, $M_o = 0.60$, (fig. 18(c)) the twisting-moment parameter increases as expected from $C_N = 0.2$ to $C_N = 0.4$. As the angle of attack is further increased, the stations inboard of $\frac{y}{b/2} = 0.7$ show a decreasing twisting-moment parameter which indicates a forward movement of the center of pressure. This forward movement of the center of pressure is associated with the formation of extensive local supersonic regions on the forward portion of the upper surface of the airfoil, as previously discussed. The influence of mid-semispan stall is again noted and occurs for the 0.915 normal-force distribution.

Root twisting-moment coefficients.- The wing root twisting-moment coefficients presented in figure 19 are referenced to a line perpendicular to the 25-percent position of the root chord. This point was arbitrarily selected as a point of interest for the structural design of the wing-root section and attachment. There is a slight Mach number effect on the root twisting-moment coefficient for angles of attack below 5° (in the subcritical range); the effect, however, is much less than that based on the Glauert factor $\frac{1}{\sqrt{1 - M_o^2}}$. At angles of attack above 5°, the

twisting-moment coefficient for a Mach number of 0.60 undergoes a large decrease due to the forward movement of the center of pressure resulting from the local regions of supersonic flow. The rapid stall at high speeds is again evidenced by the sudden rise of the root twisting-moment coefficient at an angle of attack of about 13.5°. For Mach numbers of 0.20 and 0.40, the slopes of the curves of root twisting-moment coefficient against angle of attack undergo decreases at the higher angles of attack corresponding to similar changes in the lift curves. The gradual stall at a Mach number of 0.40 and the sharp stall at a Mach number of 0.20 can be seen from this figure.

CONCLUSIONS

Tests of a 12-foot-span wing having 16-percent-thick NACA 66-series sections, 2:1 taper ratio, and an aspect ratio of 6 have been conducted in the Langley 16-foot high-speed tunnel up to a Mach number of 0.69 and indicate the following conclusions:

1. The maximum lift coefficient increases from a value of 1.07 at a Mach number of 0.15 to a peak value of 1.135 at a Mach number of 0.25 and a Reynolds number of 3,500,000, then decreases, more rapidly at first, to a value of 0.895 at a Mach number of 0.50, after which it increases very rapidly to a value of 1.10 at a Mach number of 0.60 (limit of the maximum-lift tests). At the lower Mach numbers serious losses in maximum lift coefficient were found to result from premature transition of the laminar boundary layer to a turbulent boundary layer caused by leading-edge roughness.

2. The leading-edge radius has a significant effect on the maximum-lift characteristics of airfoils at the higher Mach numbers. The rapid rise of the maximum lift coefficient for the NACA 66-series wing is attributed primarily to the unusually high acceleration of the flow around the sharp leading edge of the wing and to the rearward movement of the shock formation on the upper surface of the wing.

3. No significant changes in span load distribution and root bending-moment coefficients occurred throughout the Mach number range for all angles of attack below the stall. For all Mach numbers investigated, the spanwise distribution of normal loads on the wing can be predicted adequately for most structural purposes.

4. Extensive local supersonic-flow regions are formed over the upper surface of the wing; peak local Mach numbers of about 1.75 are obtained for a free-stream Mach number of 0.55 and an angle of attack of 13.2°.

5. The effect of the formation of the extensive local supersonic-flow regions over the upper surface of the wing is to move the center of pressure forward and reduce the section twisting-moment and root twisting-moment coefficients for given normal-force coefficients.

Langley Aeronautical Laboratory
National Advisory Committee for Aeronautics
Langley Field, Va., April 12, 1948

REFERENCES

1. Muse, Thomas C.: Some Effects of Reynolds and Mach Numbers on the Lift of an NACA 0012 Rectangular Wing in the NACA 19-Foot Pressure Tunnel. NACA CB No. 3E29, 1943.

2. Cleary, Harold E.: Effects of Compressibility on Maximum Lift Coefficients for Six Propeller Airfoils. NACA ACR No. L4L21a, 1945.

3. Nissen, James M., and Gadeberg, Burnett L.: Effect of Mach and Reynolds Numbers on the Power-Off Maximum Lift Coefficient Obtainable on a P-39N-1 Airplane as Determined in Flight. NACA ACR No. 4F28, 1944.

4. Rhode, Richard V.: Correlation of Flight Data on Limit Pressure Coefficients and Their Relation to High-Speed Burbling and Critical Tail Loads. NACA ACR No. L4I27, 1944.

5. Pearson, E. O., Jr., Evans, A. J., and West, F. E., Jr.: Effects of Compressibility on the Maximum Lift Characteristics and Spanwise Load Distribution of a 12-Foot-Span Fighter-Type Wing of NACA 230-Series Airfoil Sections. NACA ACR No. L5G10, 1945.

6. Pearson, E. O., Jr.: Effect of Compressibility on the Distribution of Pressures over a Tapered Wing of NACA 230-Series Airfoil Sections. NACA TN No. 1390, 1947.

7. Furlong, G. Chester, and Fitzpatrick, James E.: Effects of Mach Number and Reynolds Number on the Maximum Lift Coefficient of a Wing of NACA 230-Series Airfoil Sections. NACA TN No. 1299, 1947.

8. Swanson, Robert S., and Gillis, Clarence L.: Wind-Tunnel Calibration and Correction Procedures for Three-Dimensional Models. NACA ARR No. L4E31, 1944.

9. Goldstein, S., and Young, A. D.: The Linear Perturbation Theory of Compressible Flow, with Applications to Wind-Tunnel Interference. R. & M. No. 1909, British A.R.C., 1943.

10. Lotz, Irmgard: Correction of Downwash in Wind Tunnels of Circular and Elliptic Sections. NACA TM No. 801, 1936.

11. Thom, A.: Blockage Corrections in a Closed High-Speed Tunnel. R. & M. No. 2033, British A.R.C., 1943.

12. Spreiter, John R., and Steffen, Paul J.: Effect of Mach and Reynolds Numbers on Maximum Lift Coefficient. NACA TN No. 1044, 1946.

13. Wall, Nancy E.: Chordwise Pressure Distributions on a 12-Foot-Span Wing of NACA 66-Series Airfoil Sections up to a Mach Number of 0.60. NACA TN No. 1696, 1948.

14. Anon.: Spanwise Air-Load Distribution. ANC-1(1), Army-Navy-Commerce Committee on Aircraft Requirements. U.S. Govt. Printing Office, April 1938.

15. Abbott, Ira H., Von Doenhoff, Albert E., and Stivers, Louis S., Jr.: Summary of Airfoil Data. NACA Rep. No. 824, 1945.

16. Neely Robert H., and Foster, Gerald V.: Wind-Tunnel Investigation of an NACA 66-Series 16-Percent-Thick Low-Drag Tapered Wing with Fowler and Split Flaps. NACA ACR No. L5F28, 1946.

17. Sivells, James C.: Experimental and Calculated Characteristics of Three Wings of NACA 64-210 and 65-210 Airfoil Sections with and without 2° Washout. NACA TN No. 1422, 1947.

18. Göthert, B.: Plane and Three-Dimensional Flow at High Subsonic Speeds. NACA TM No. 1105, 1946.

19. Lindsey, W. F., Daley, Bernard N., and Humphreys, Milton D.: The Flow and Force Characteristics of Supersonic Airfoils at High Subsonic Speeds. NACA TN No. 1211, 1947.

TABLE I

AIRFOIL ORDINATES OF 66-SERIES WING

[Stations and ordinates are given in percent of airfoil chord]

Root section				Tip section			
Upper surface		Lower surface		Upper surface		Lower surface	
Station	Ordinate	Station	Ordinate	Station	Ordinate	Station	Ordinate
0	0	0	0	0	0	0	0
.43	1.21	.57	-1.15	.37	1.24	.63	-1.11
.68	1.46	.82	-1.37	.61	1.50	.89	-1.32
1.17	1.82	1.33	-1.68	1.09	1.89	1.41	-1.61
2.41	2.50	2.59	-2.25	2.32	2.61	2.68	-2.13
4.90	3.50	5.10	-3.08	4.79	3.70	5.21	-2.87
7.39	4.28	7.61	-3.73	7.28	4.56	7.72	-3.44
9.89	4.97	10.11	-4.28	9.78	5.31	10.22	-3.93
14.89	6.05	15.11	-5.15	14.79	6.50	15.21	-4.70
19.90	6.89	20.10	-5.83	19.81	7.43	20.19	-5.29
24.92	7.55	25.08	-6.34	24.83	8.16	25.17	-5.74
29.93	8.05	30.07	-6.74	29.86	8.71	30.14	-6.08
34.95	8.41	35.05	-7.02	34.90	9.11	35.10	-6.32
39.97	8.63	40.03	-7.18	39.94	9.36	40.06	-6.46
44.99	8.73	45.01	-7.26	44.98	9.47	45.03	-6.52
50.01	8.69	49.99	-7.22	50.03	9.43	49.98	-6.48
55.04	8.50	54.96	-7.06	55.08	9.23	54.93	-6.34
60.07	8.11	59.93	-6.74	60.14	8.80	59.86	-6.05
65.10	7.46	64.90	-6.20	65.19	8.08	64.81	-5.58
70.10	6.52	69.90	-5.42	70.20	7.07	69.80	-4.86
75.09	5.43	74.91	-4.50	75.18	5.89	74.82	-4.03
80.08	4.23	79.93	-3.49	80.15	4.59	79.85	-3.11
85.05	2.99	84.95	-2.44	85.11	3.26	84.89	-2.17
90.03	1.76	89.97	-1.41	90.06	1.94	89.94	-1.24
95.01	.68	94.99	-.52	95.02	.76	94.98	-.43
100	0	100	0	100	0	100	0
Leading-edge radius = 1.475c Slope of radius through leading edge = 0.058				Leading-edge radius = 1.475c Slope of radius through leading edge = 0.117			

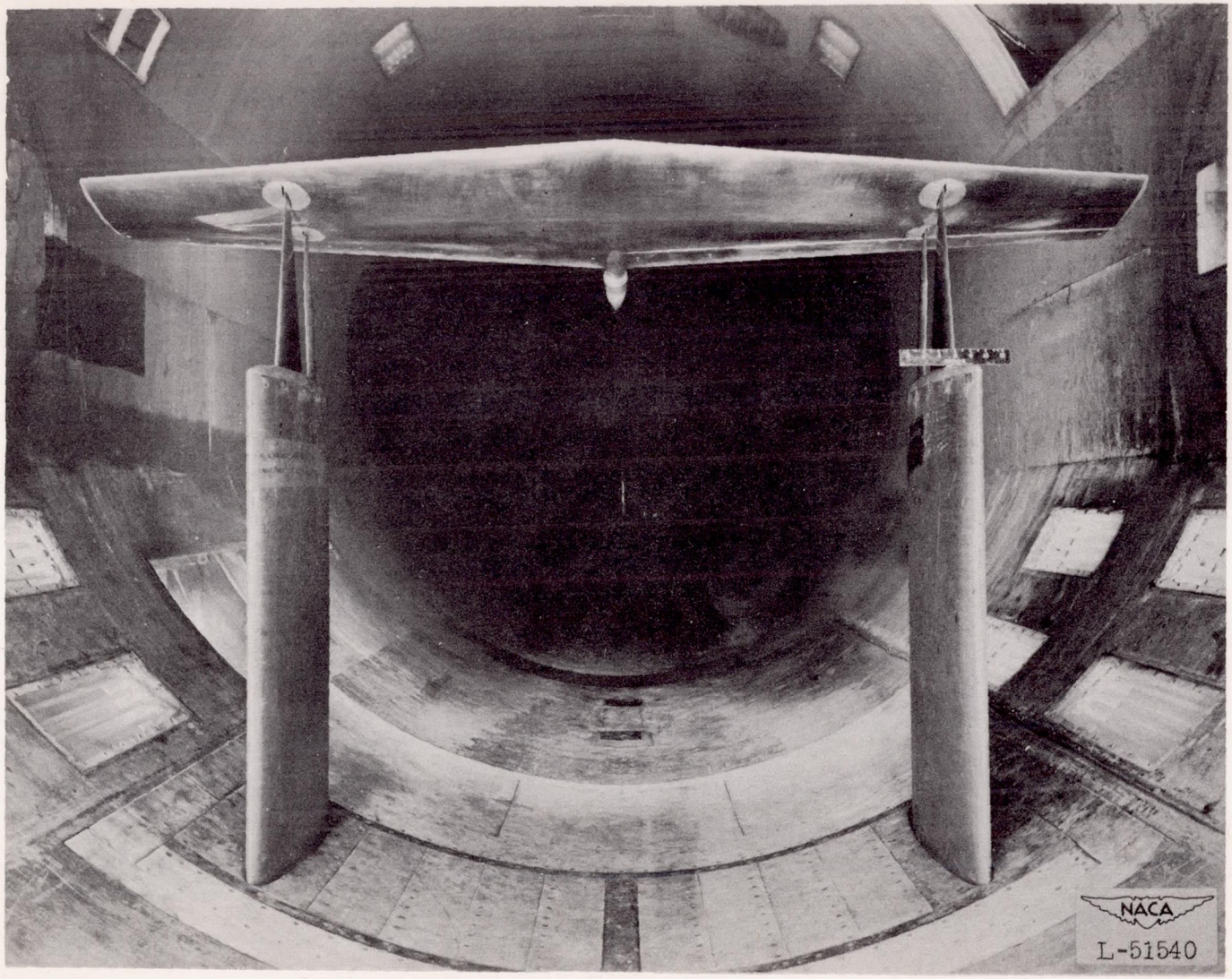

Figure 1.- Leading-edge view of test wing mounted on normal support struts.

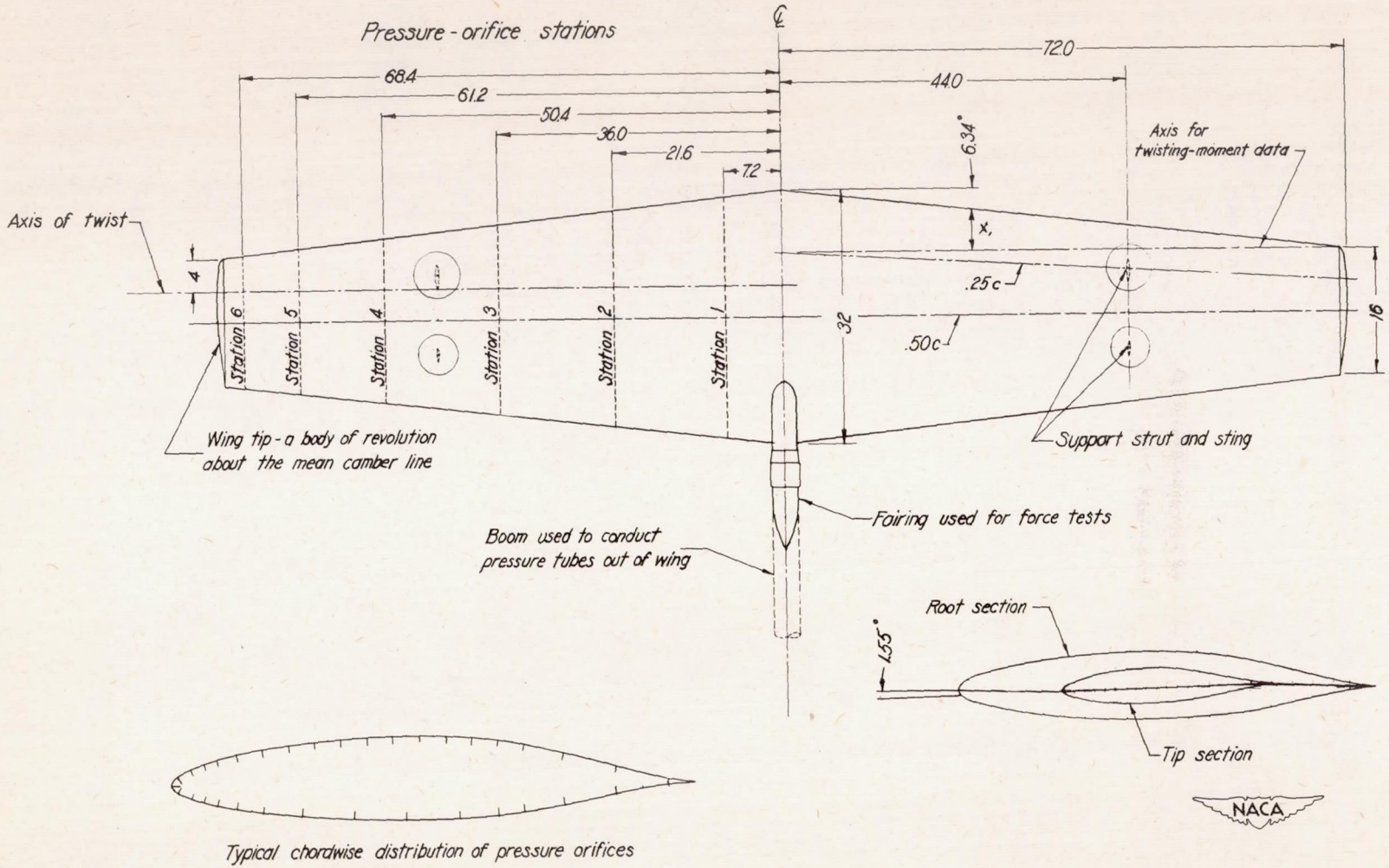

Figure 2.- Principal wing dimensions and locations of pressure orifices. (All dimensions in inches.)

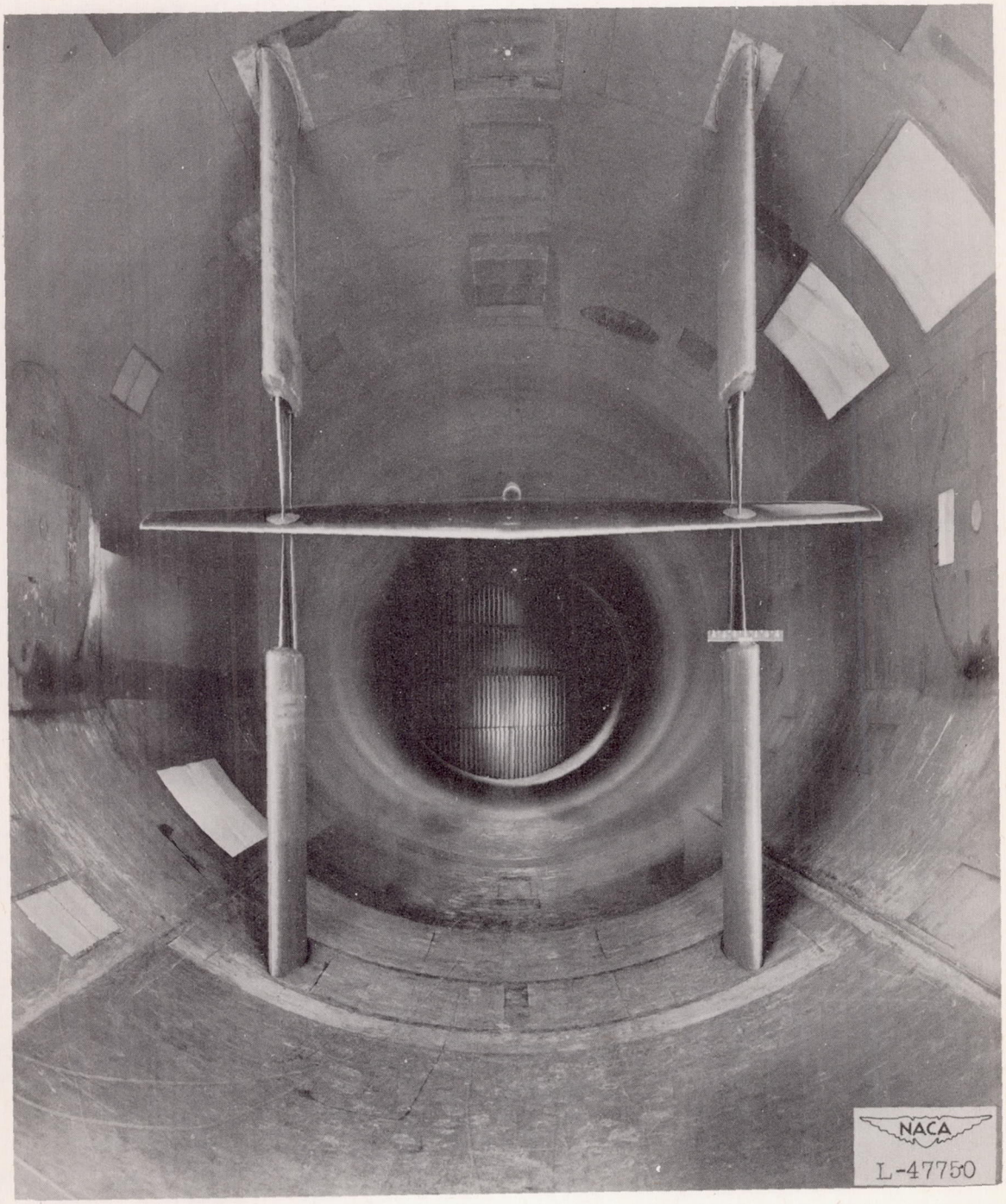

Figure 3.- Downstream view of test wing mounted on normal and image support struts.

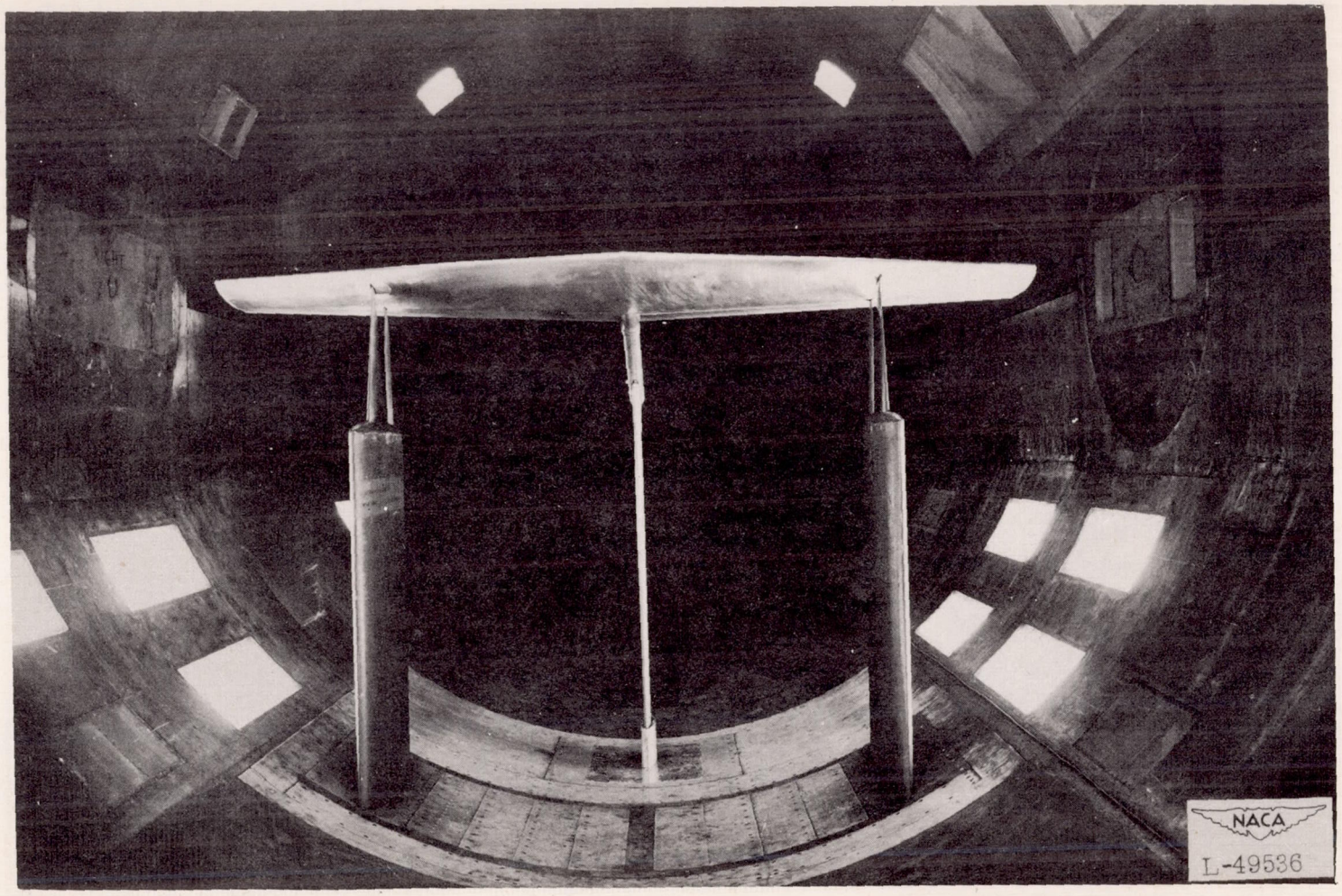

(a) Downstream view.

Figure 4.- Test wing mounted for pressure tests.

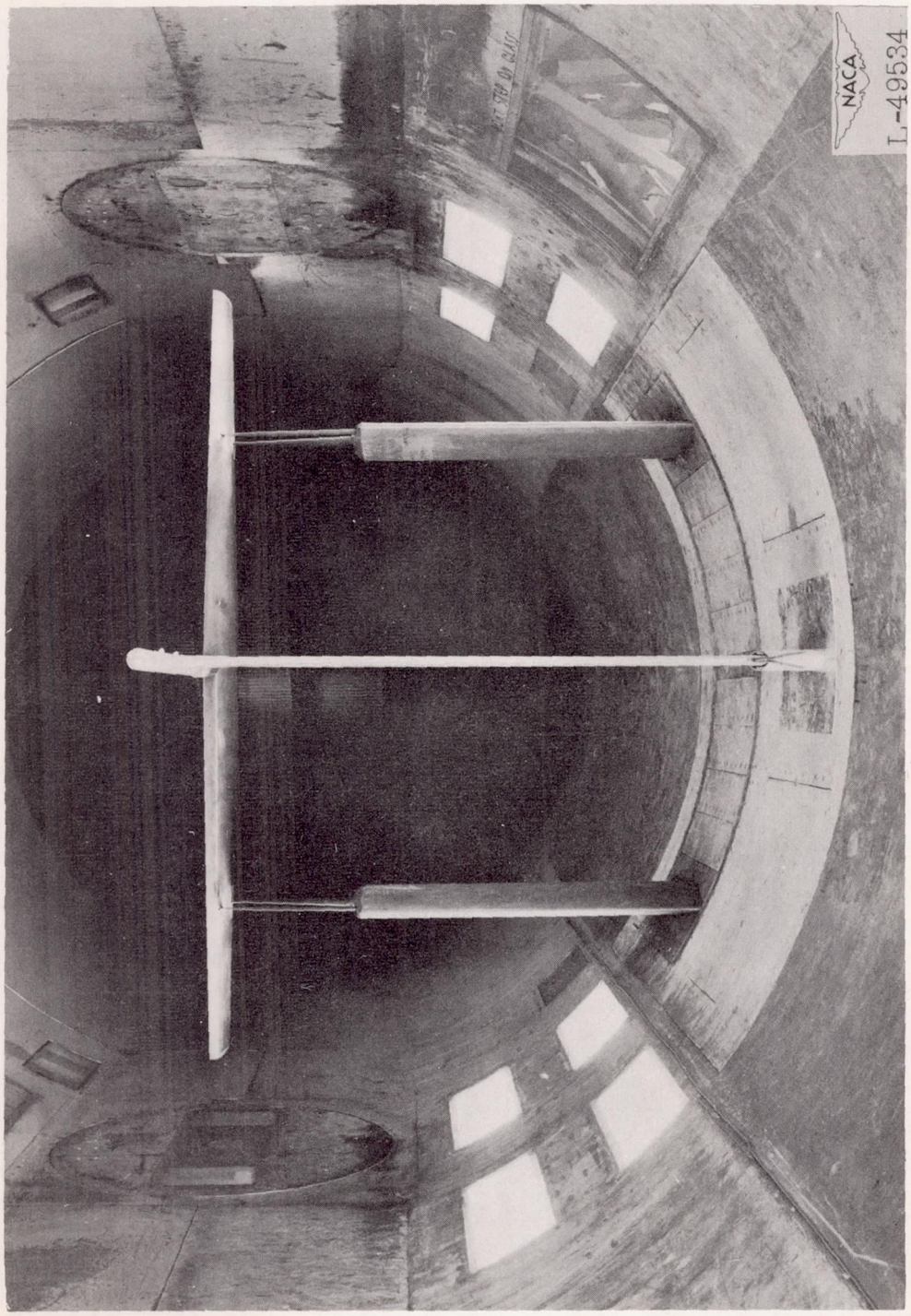

(b) Upstream view.

Figure 4.- Concluded.

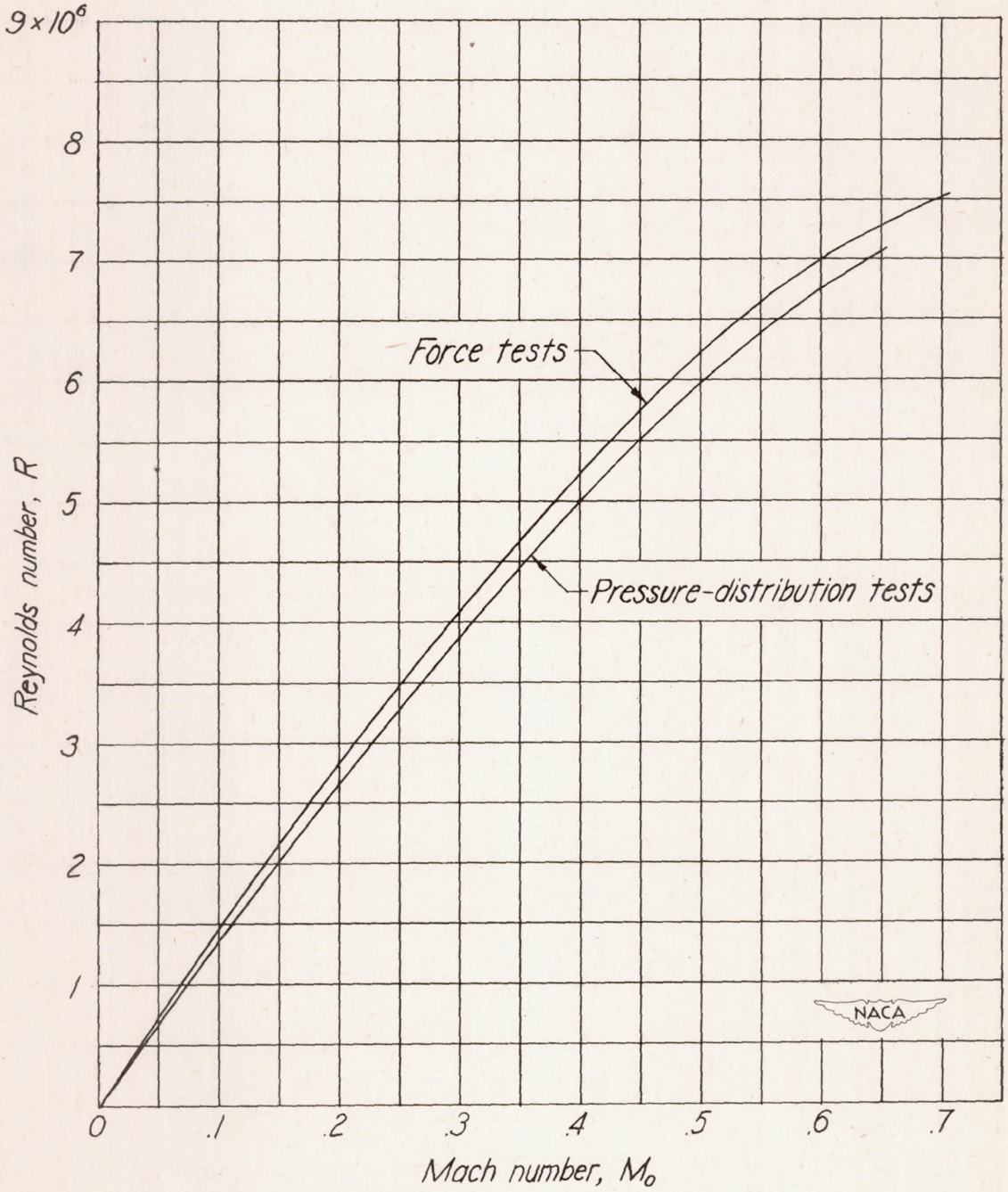

Figure 5.- Variation of average test Reynolds number with Mach number.

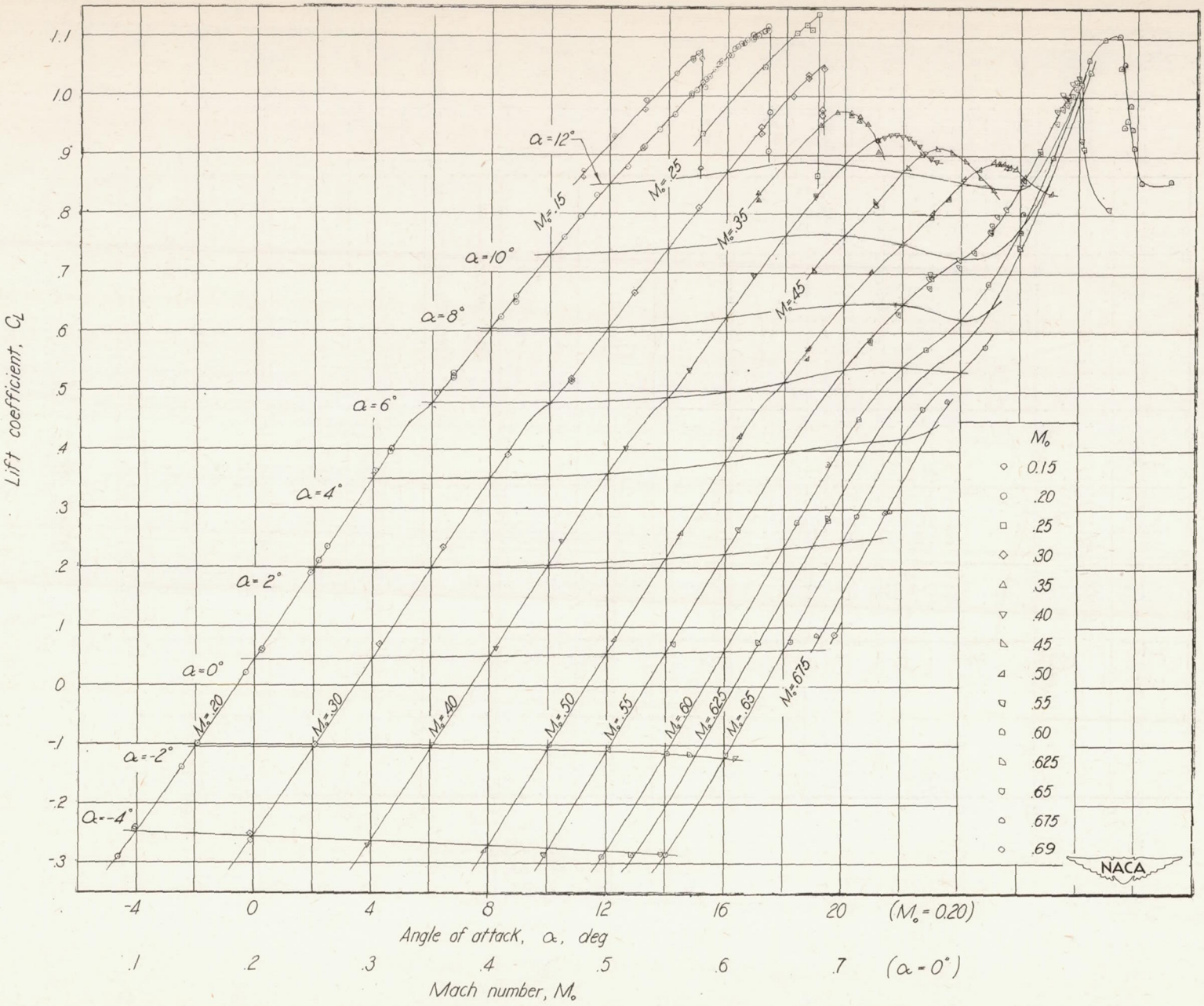

Figure 6.- Wing lift coefficient as a function of angle of attack and Mach number.

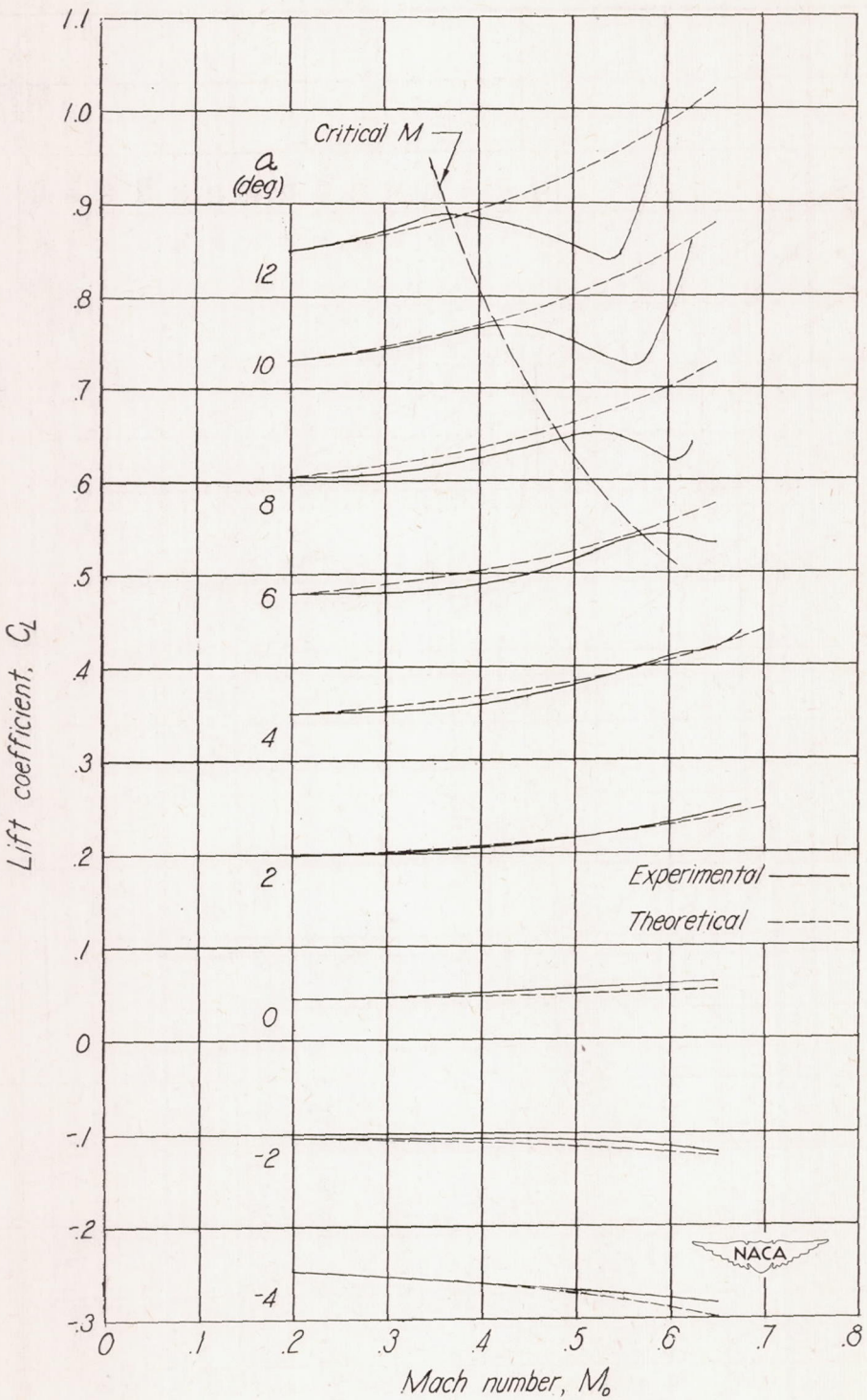

(a) α from -4° to 12°.

Figure 7.- Comparison of the experimental and theoretical variation of wing lift coefficient with Mach number.

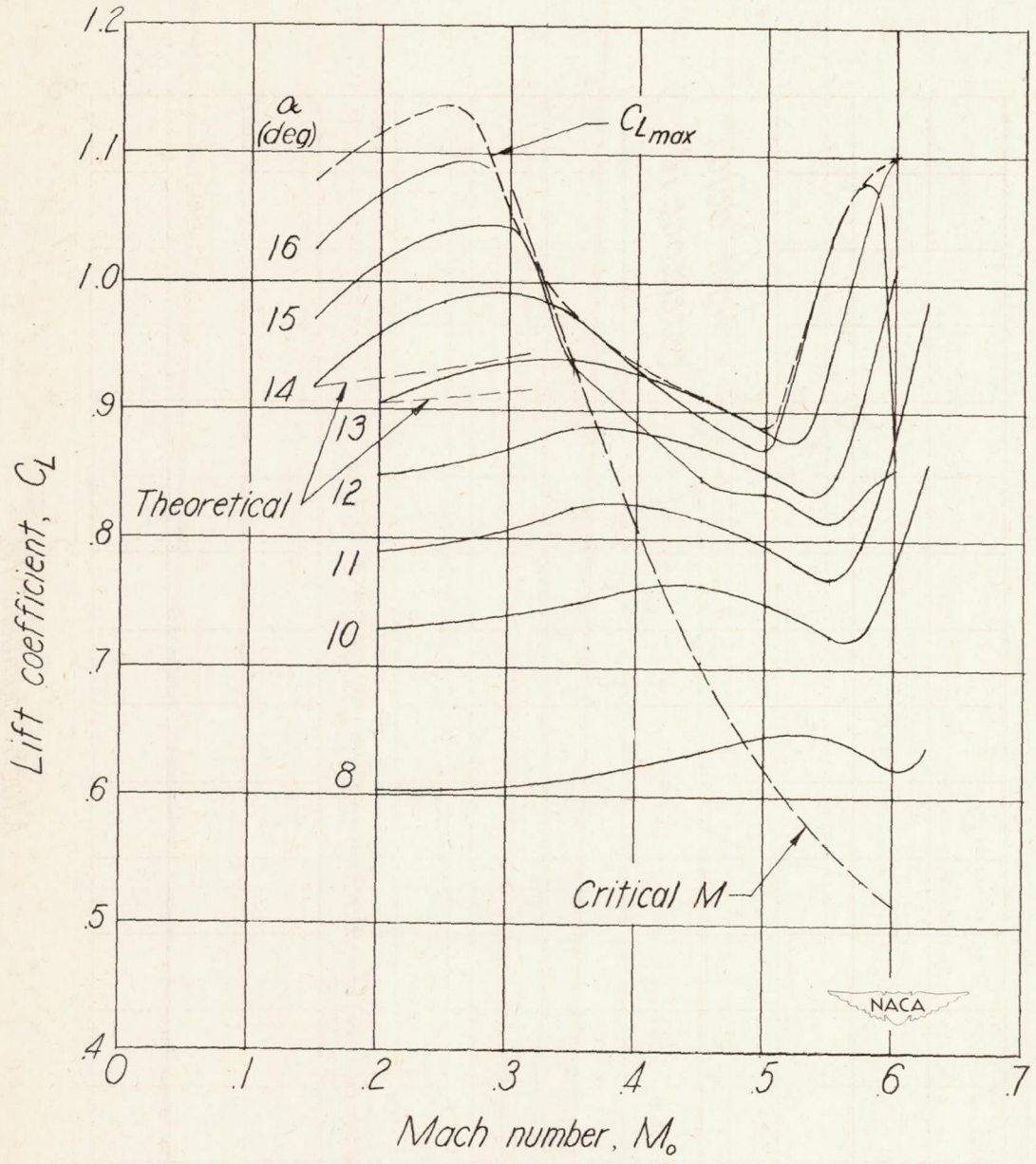

(b) α from 8° to stall.

Figure 7.- Concluded.

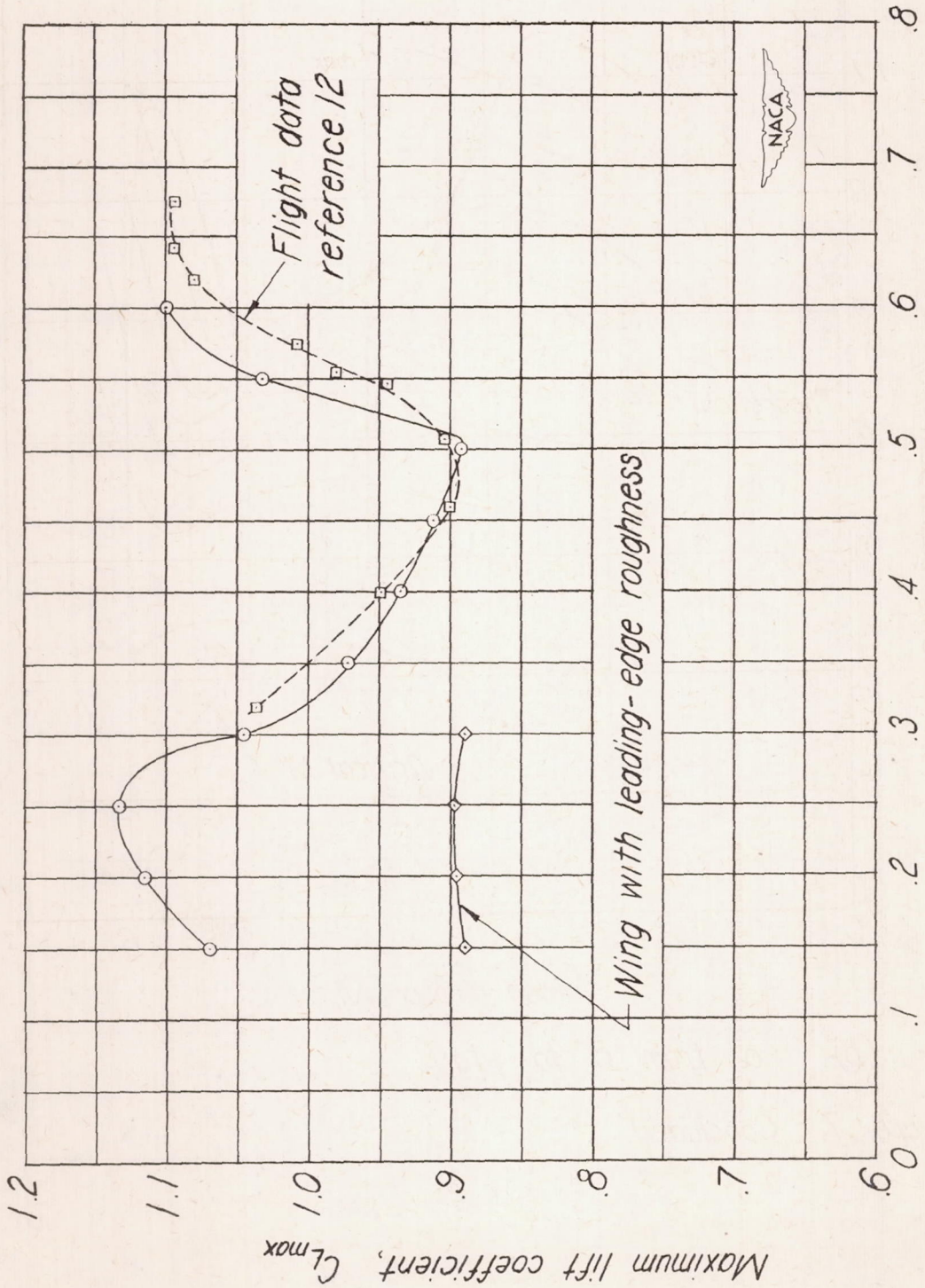

Figure 8.- Variation of maximum lift coefficient with Mach number.

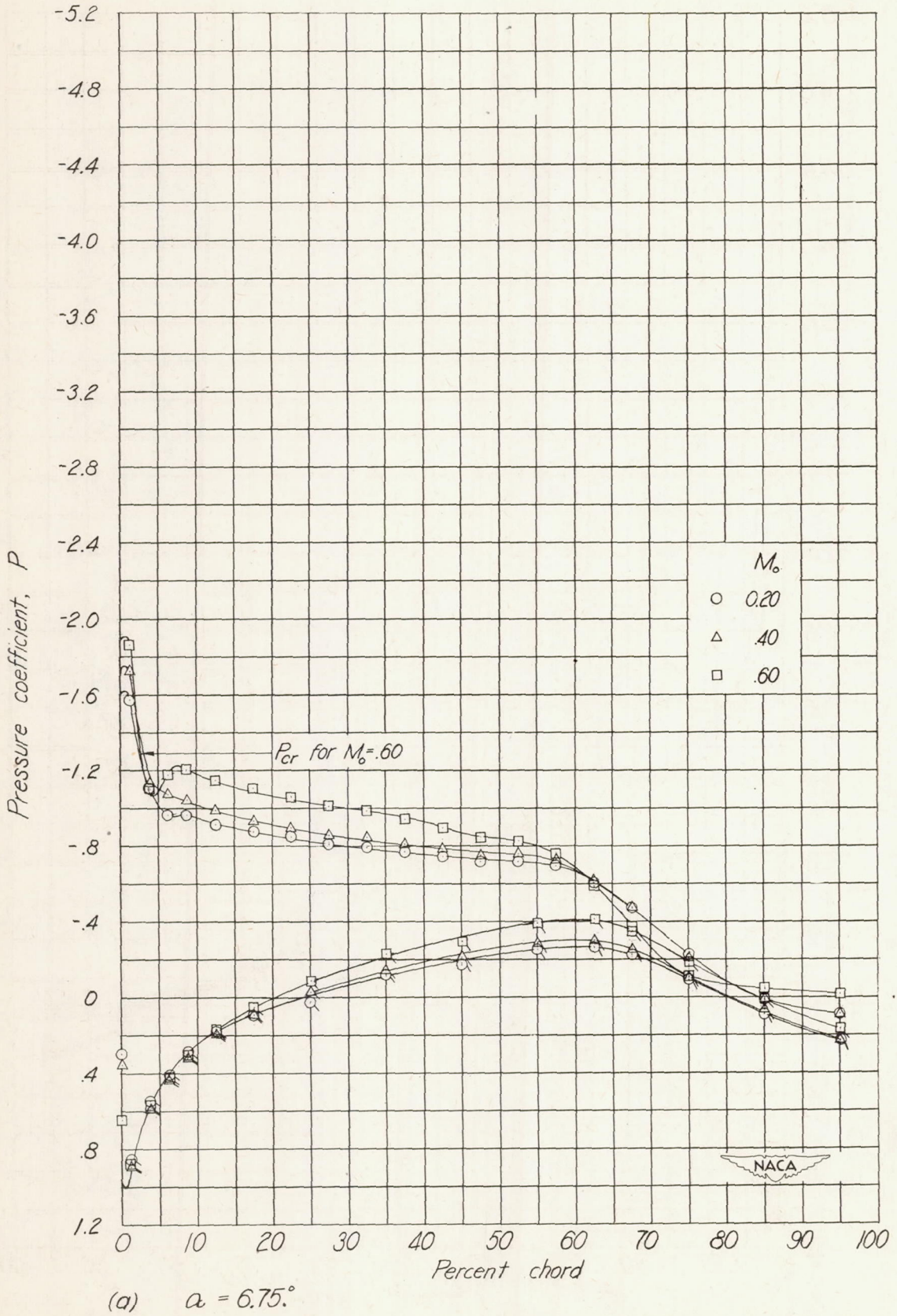

(a) $\alpha = 6.75°$

Figure 9.- Variation of section pressure distribution with Mach number at the mid-semispan station ($y/\frac{b}{2} = 0.5$) for representative angles of attack.

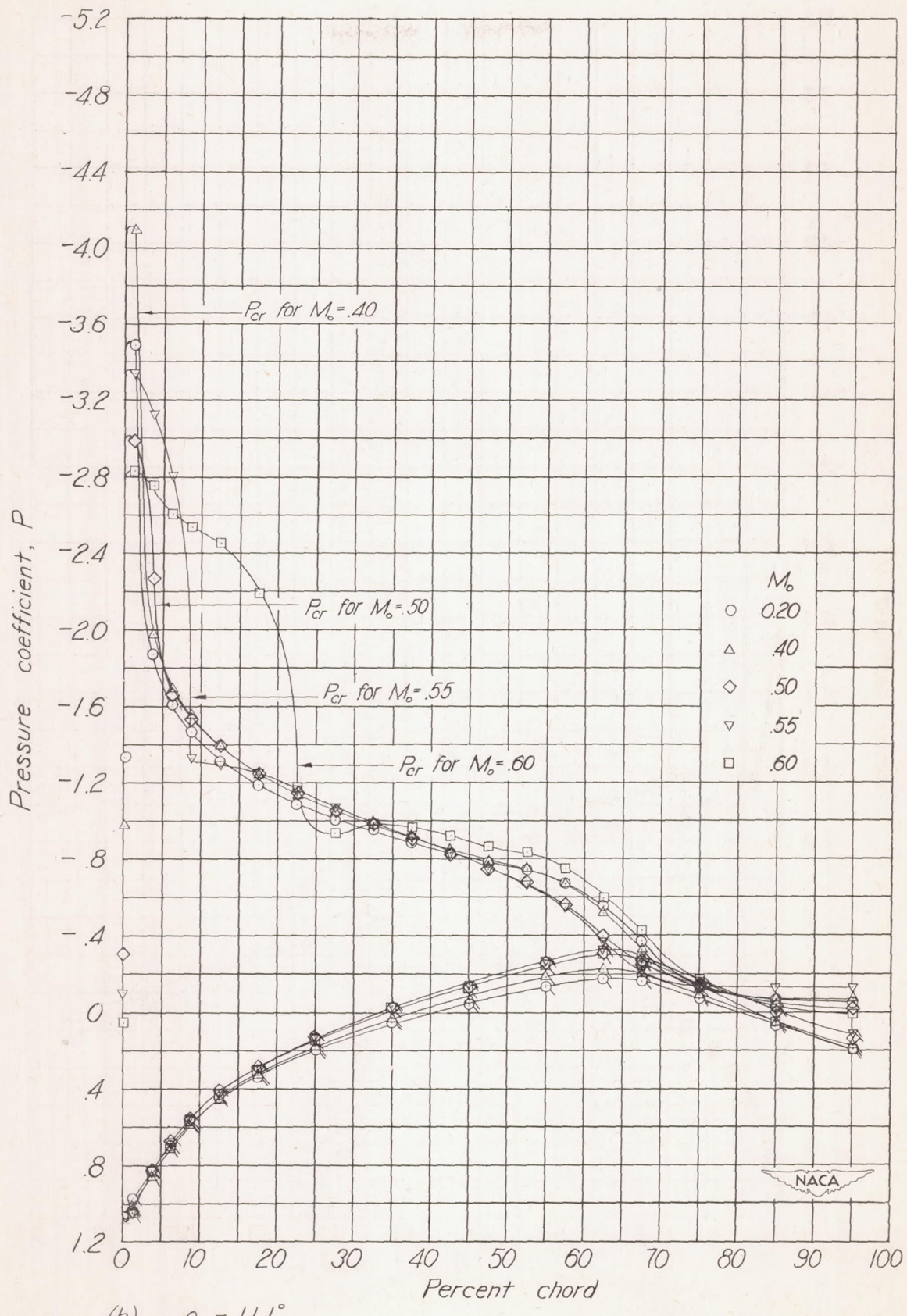

(b) $\alpha = 11.1°$.

Figure 9.- Continued.

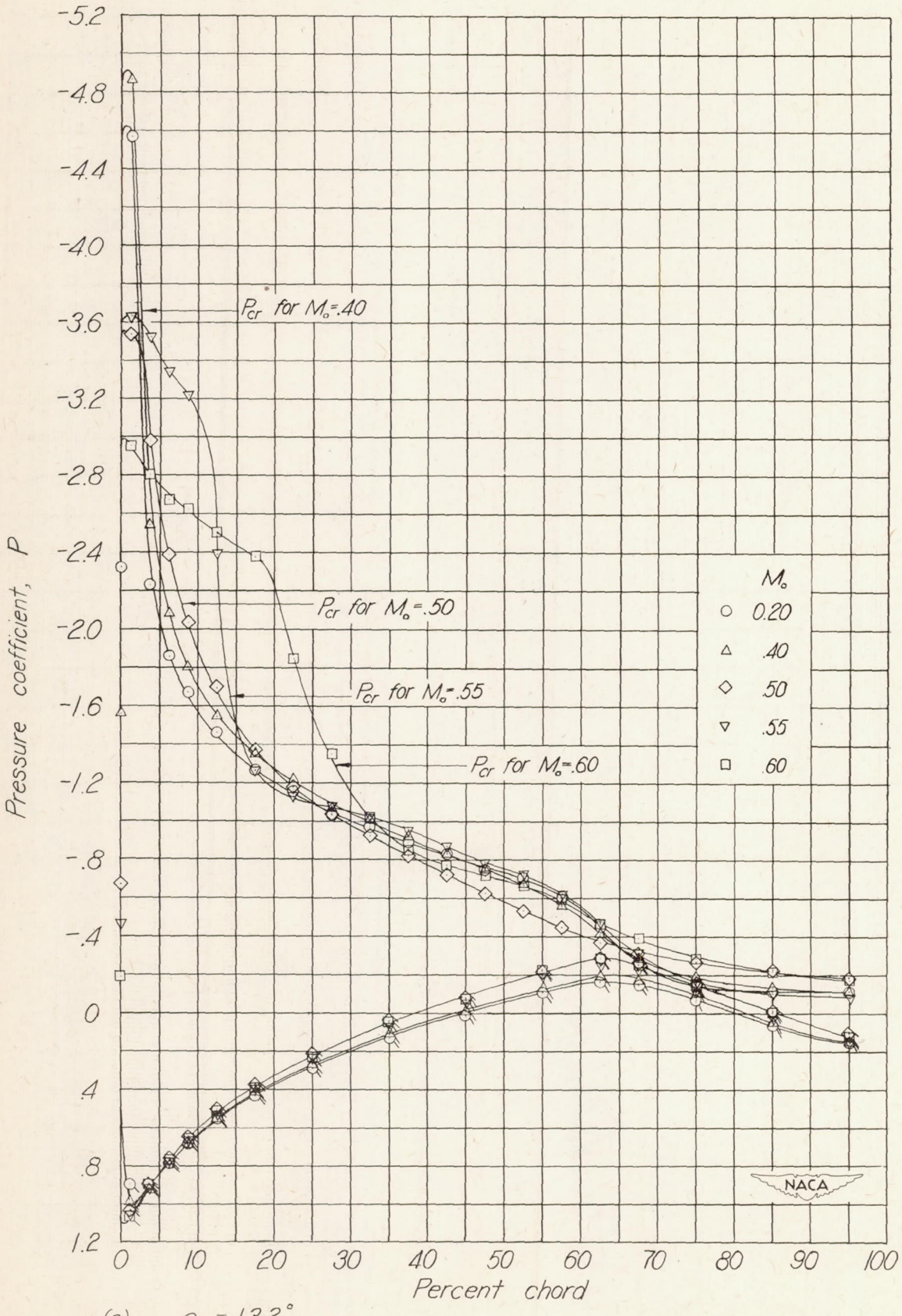

(c) $\alpha = 13.2°$.

Figure 9.- Concluded.

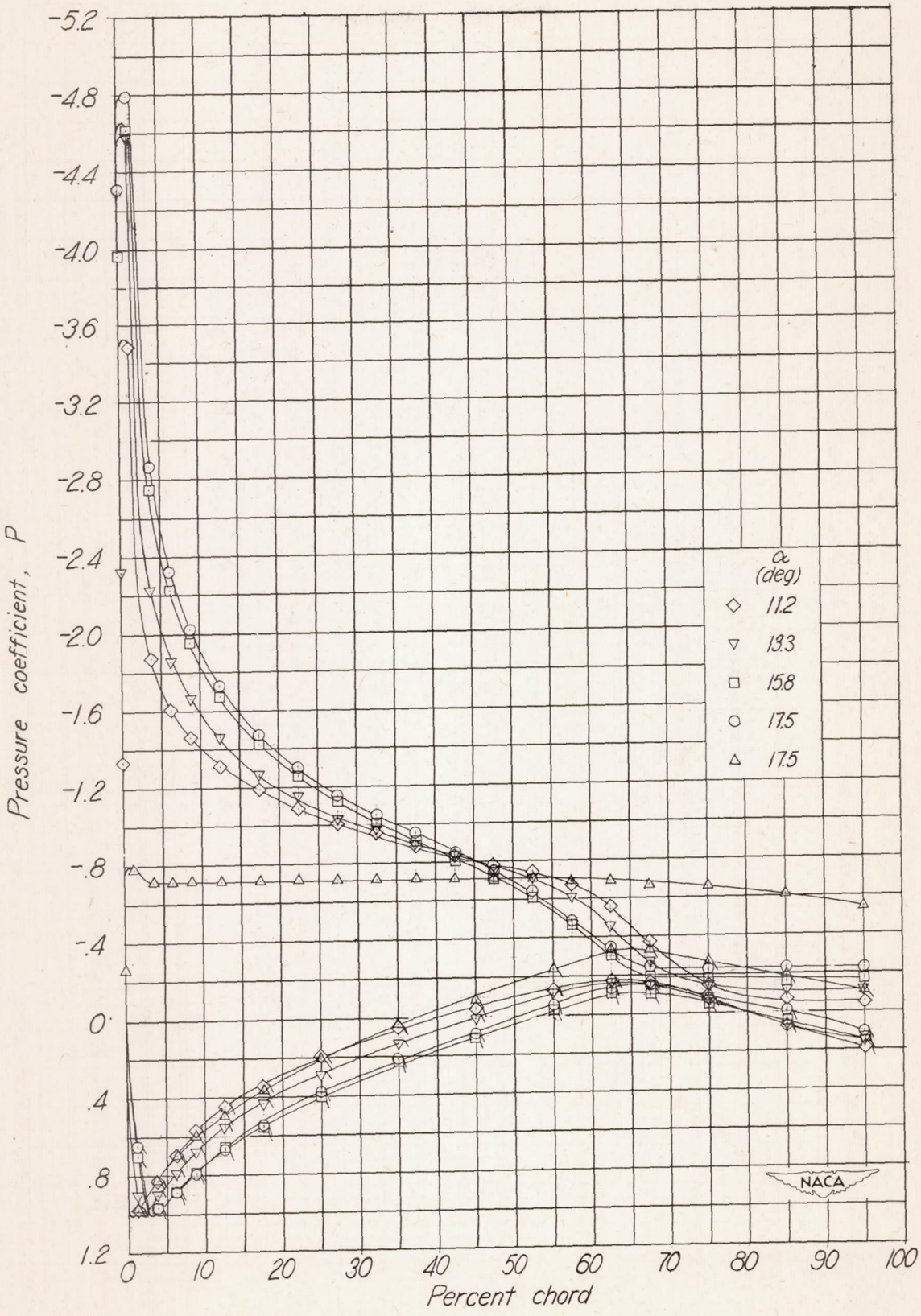

(a) $M_o = 0.20$.

Figure 10.- Variation of section pressure distribution with angle of attack at the mid-semispan station ($y/\frac{b}{2} = 0.5$) for Mach numbers of 0.20, 0.40, and 0.60.

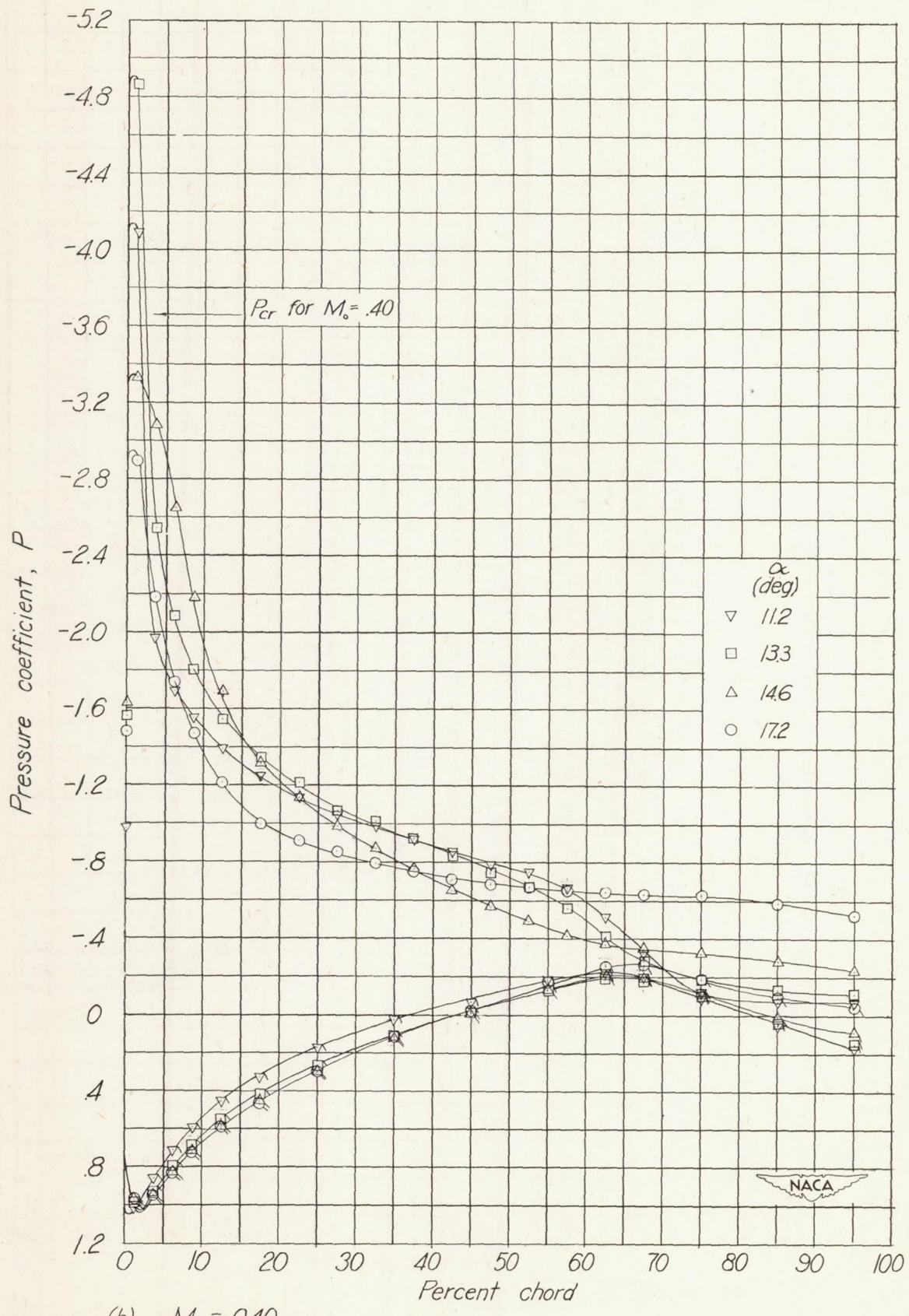

(b) M_o = 0.40.

Figure 10.- Continued.

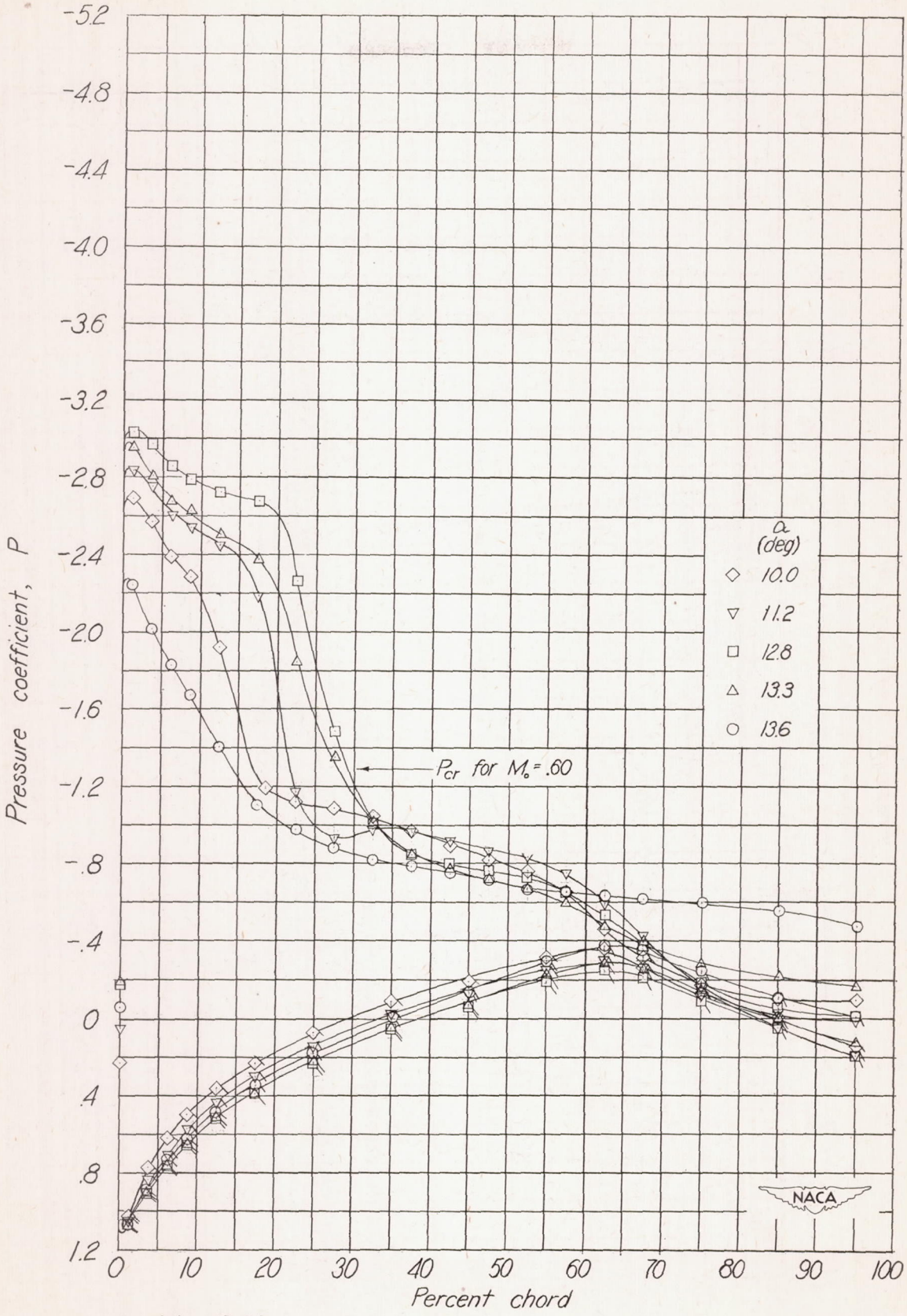

(c) M_o = 0.60.

Figure 10.- Concluded.

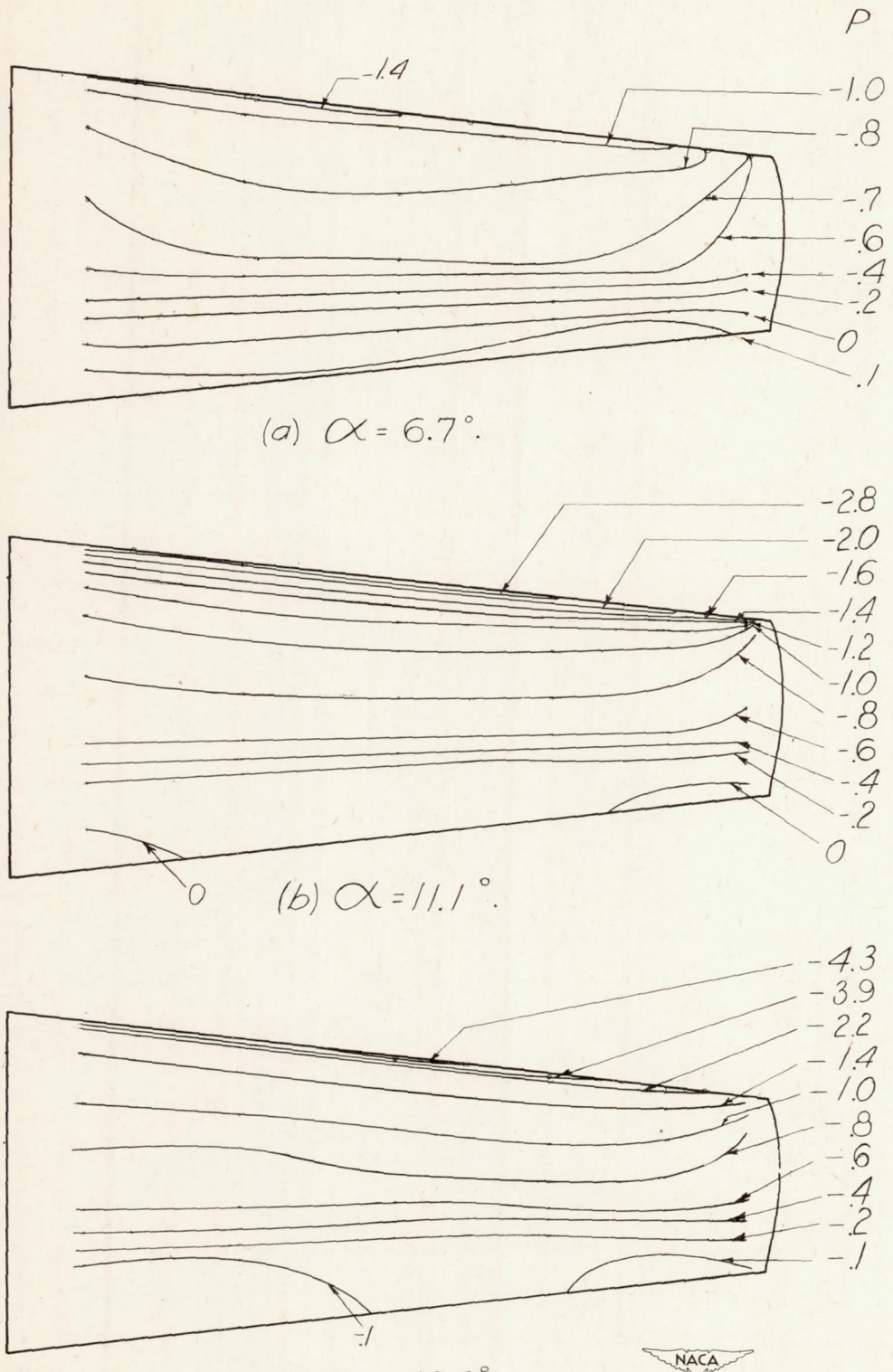

Figure 11.- Pressure contours over the upper surface of the wing for representative angles of attack for $M_o = 0.20$.

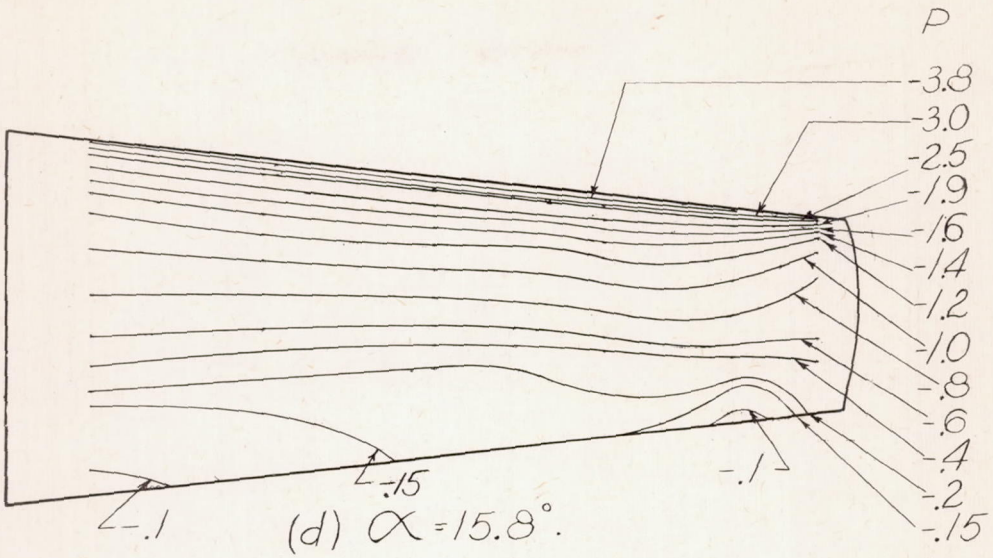

(d) $\alpha = 15.8°$.

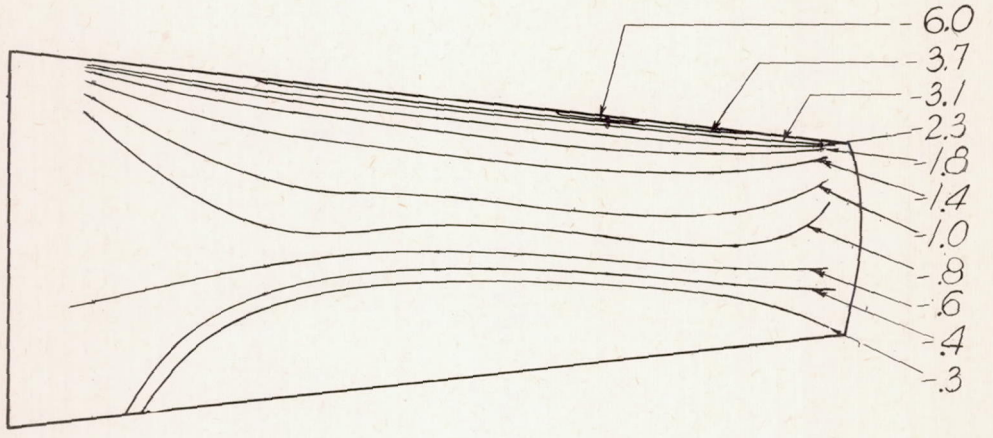

(e) $\alpha = 17.5°$.

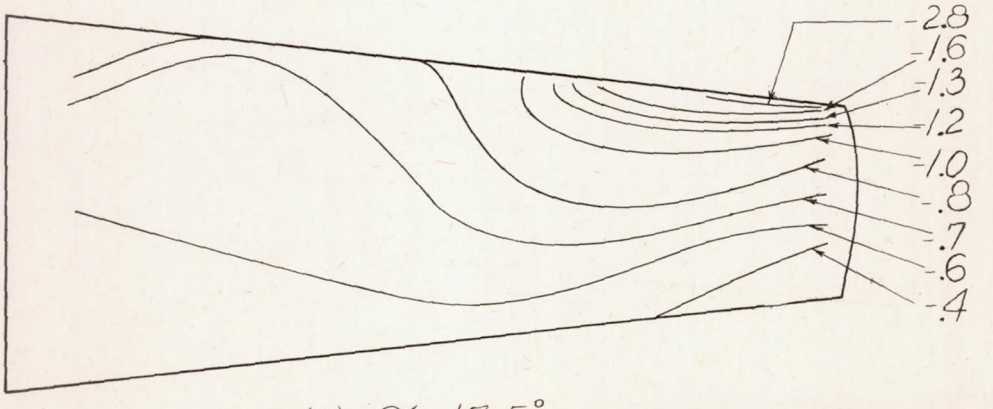

(f) $\alpha = 17.5°$.

Figure 11.- Concluded.

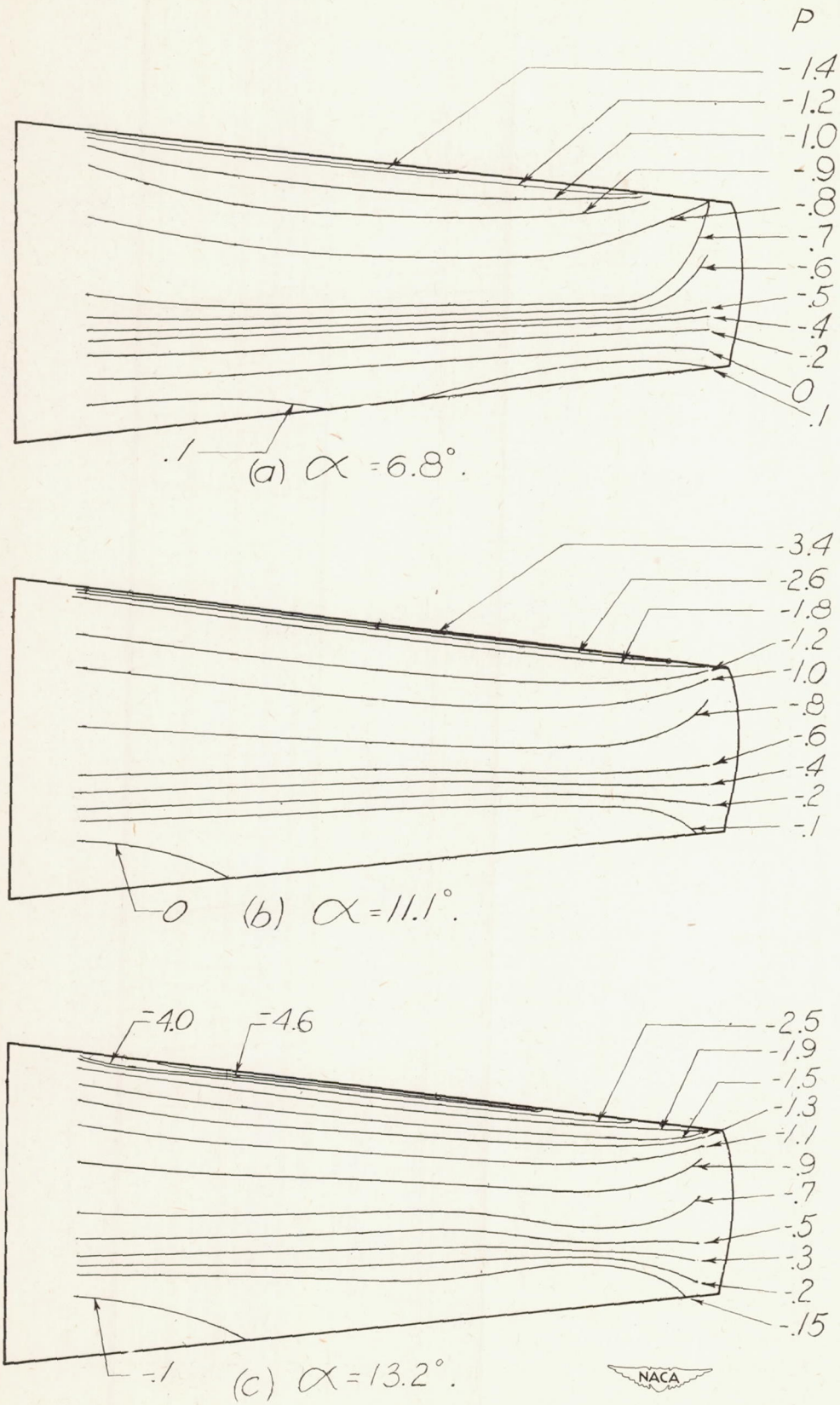

Figure 12.- Pressure contours over the upper surface of the wing for representative angles of attack for $M_o = 0.40$.

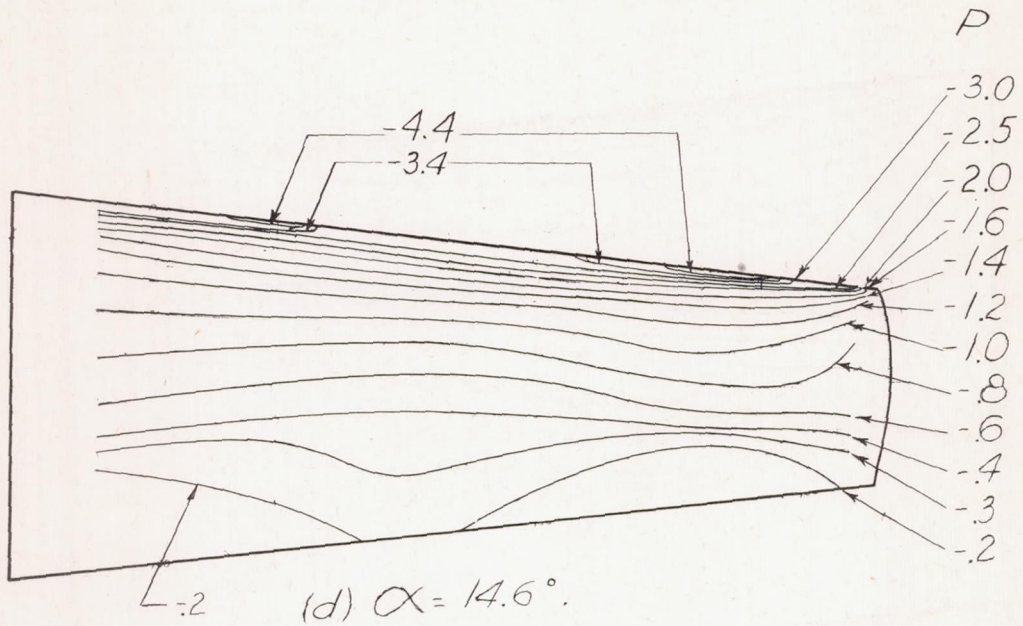

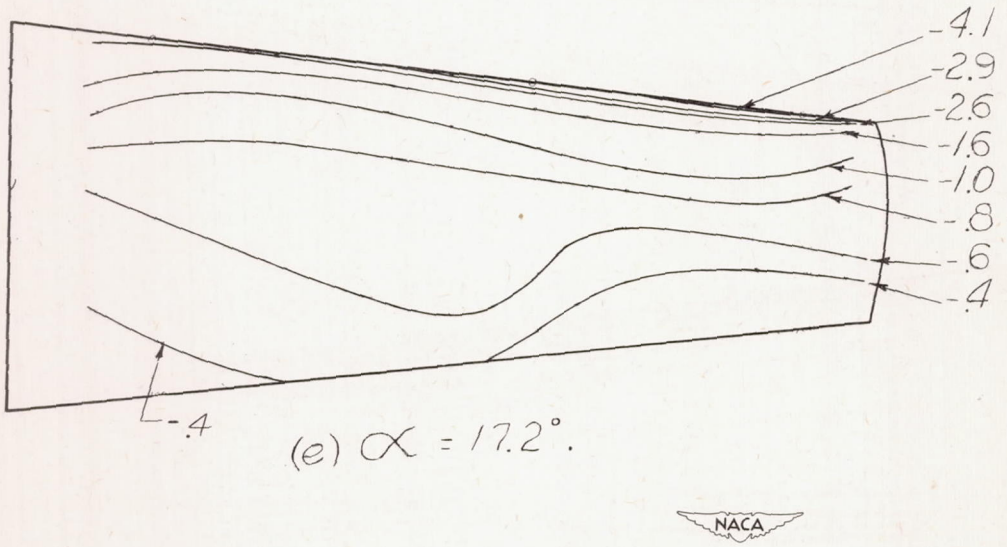

Figure 12.- Concluded.

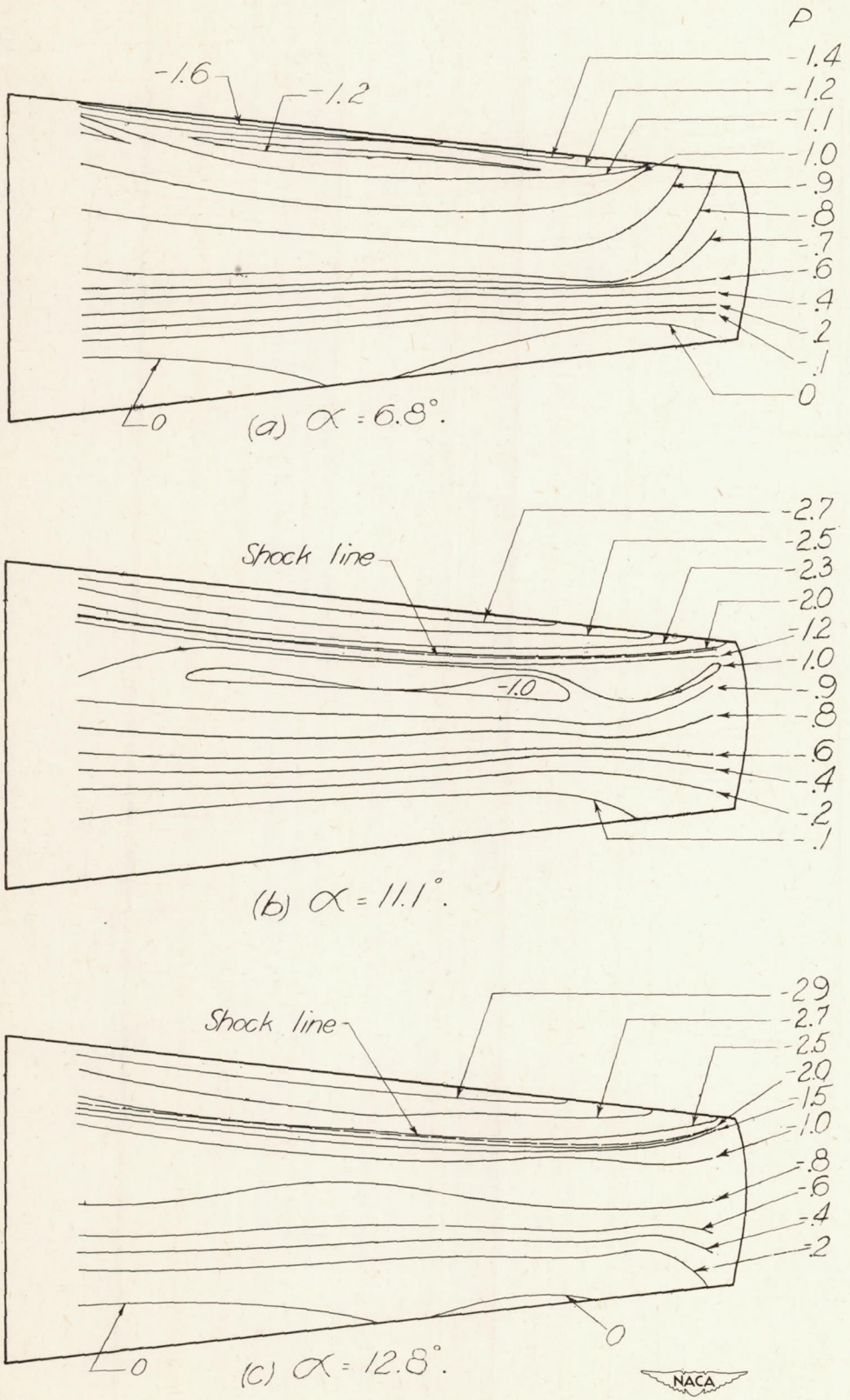

Figure 13.- Pressure contours over the upper surface of the wing for representative angles of attack for $M_o = 0.60$.

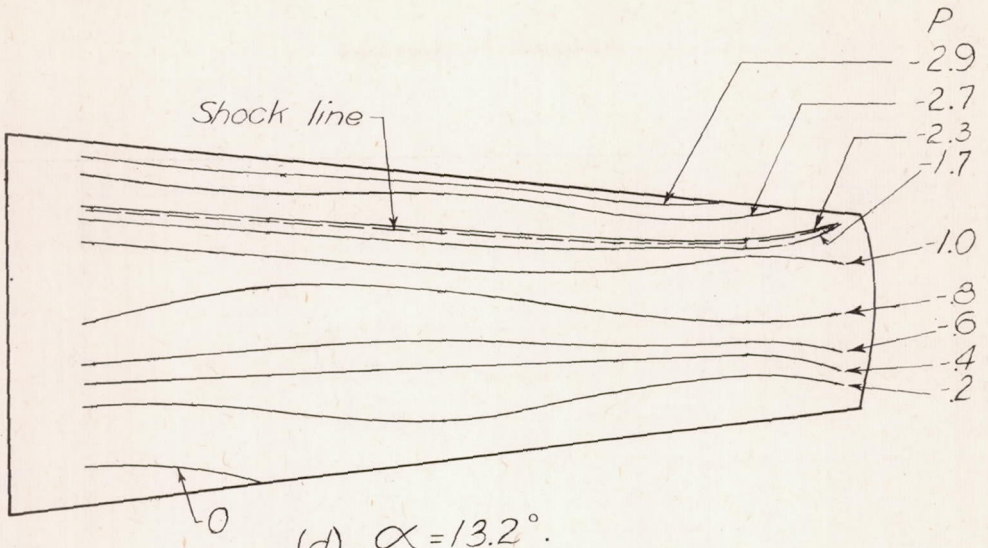

(d) $\alpha = 13.2°$.

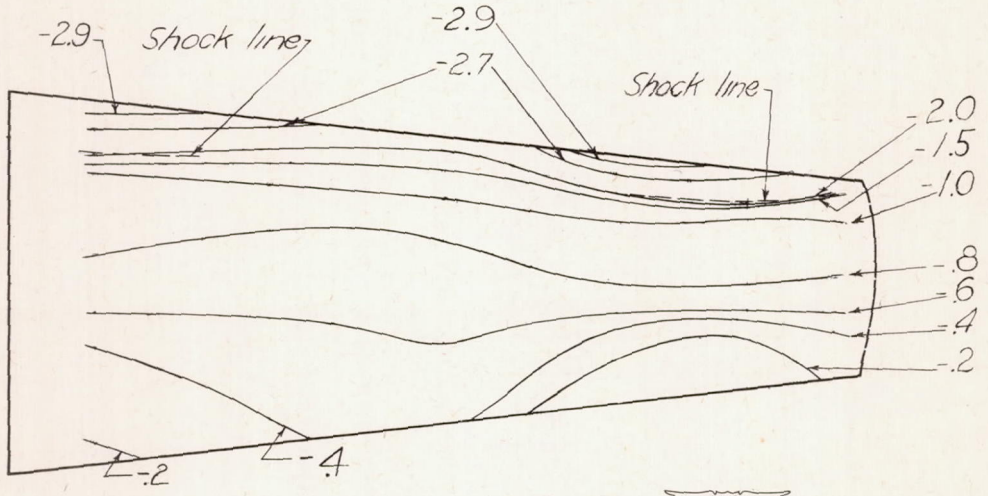

(e) $\alpha = 13.5°$.

Figure 13.- Concluded.

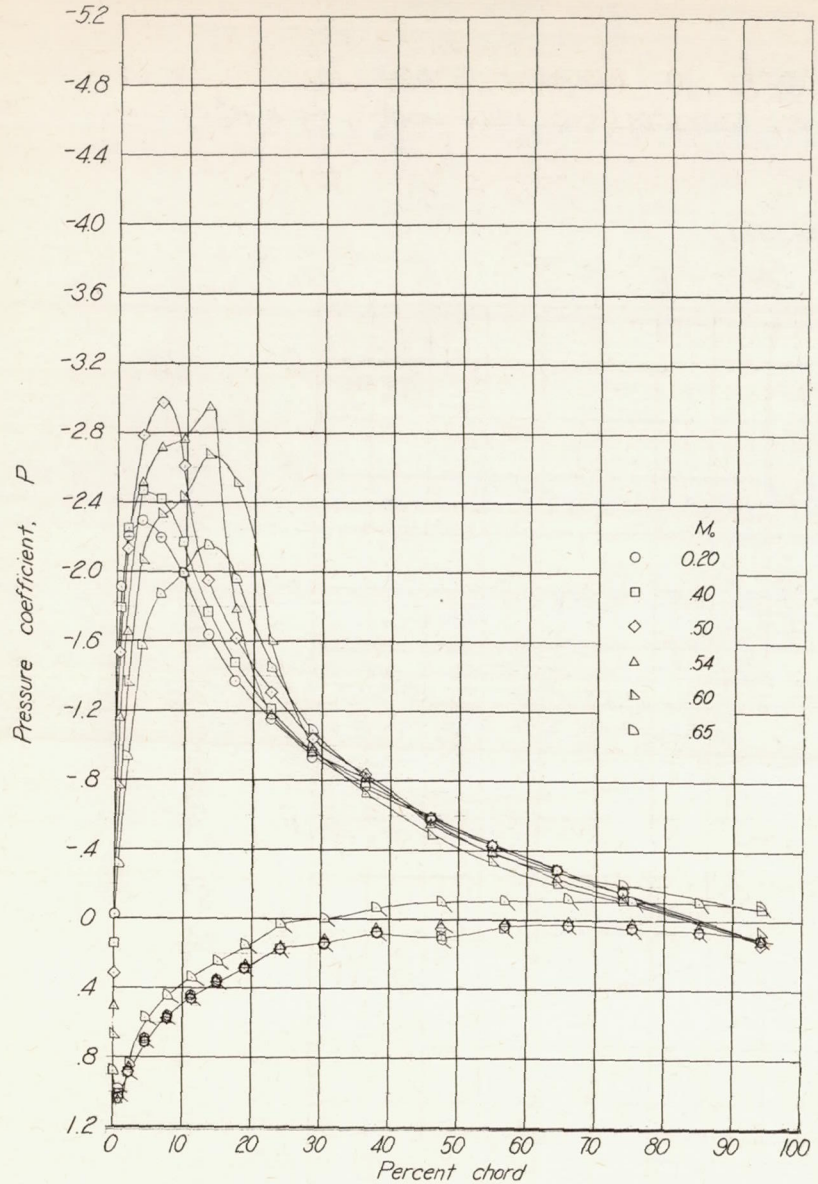

(a) NACA 230-series wing. $\alpha = 11.2°$; $\frac{y}{b/2} = 0.47$.

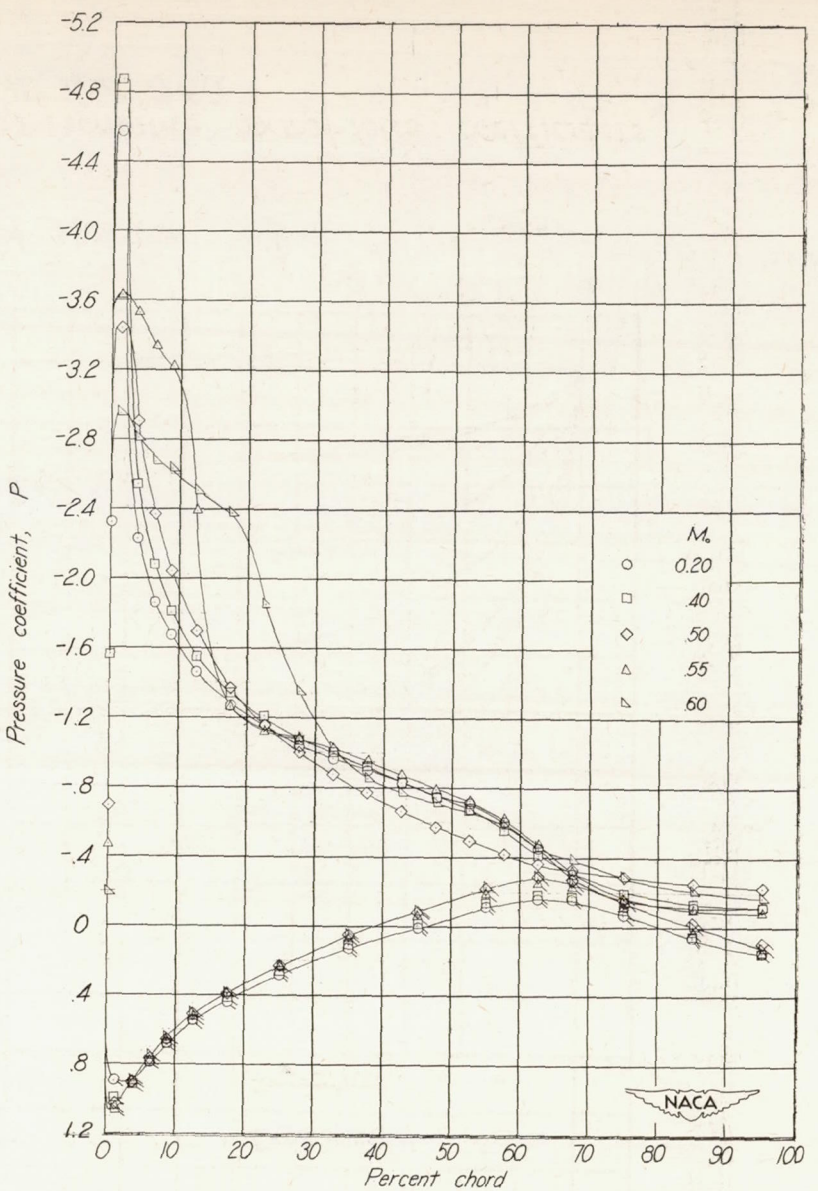

(b) NACA 66-series wing. $\alpha = 13.3°$; $\frac{y}{b/2} = 0.50$.

Figure 14.- Variation of pressure distributions with Mach number over representative sections of wings of NACA 230- and 66-series sections.

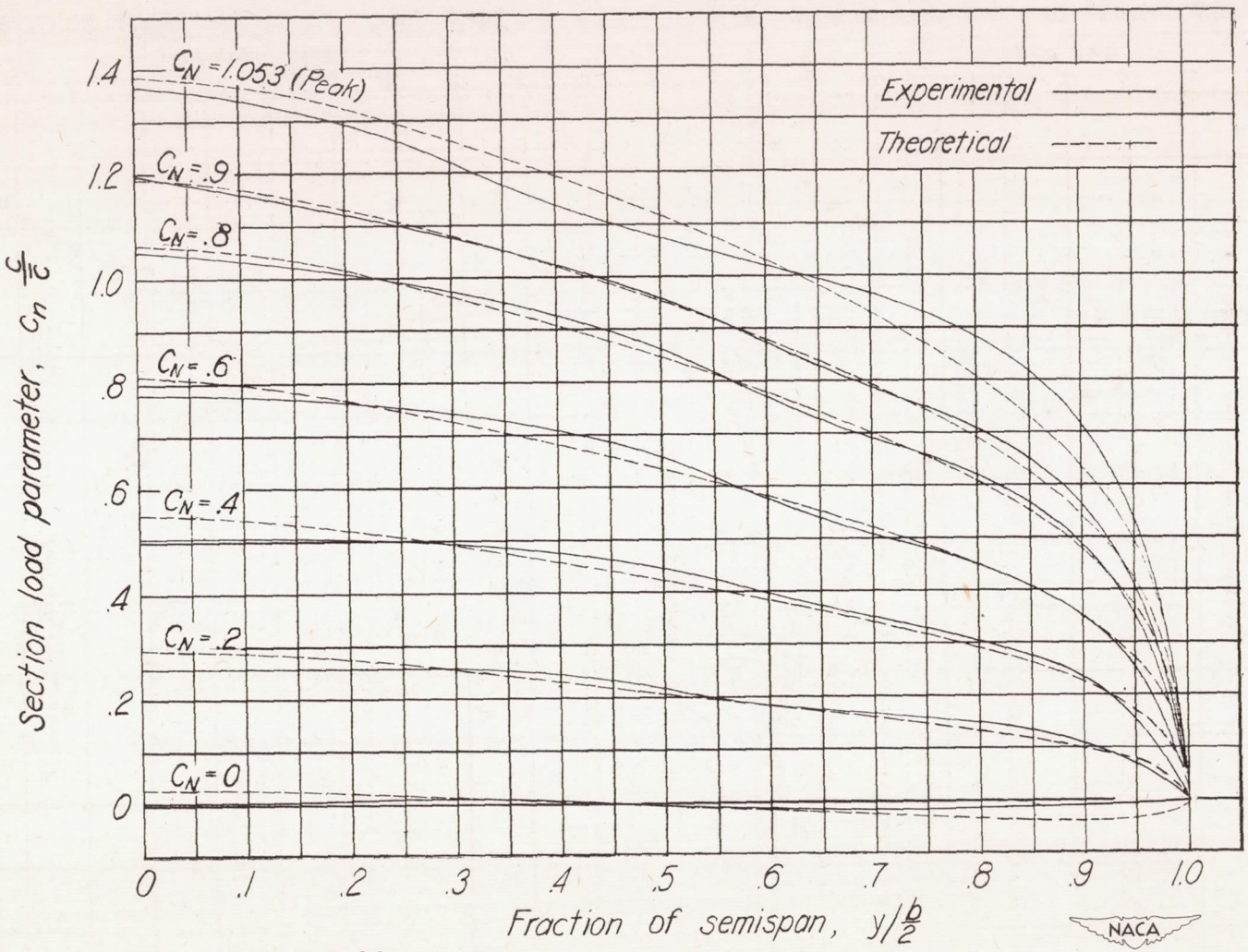

(a) M_o = 0.20.

Figure 15.- Span load distributions for representative normal-force coefficients for Mach numbers of 0.20, 0.40, and 0.60.

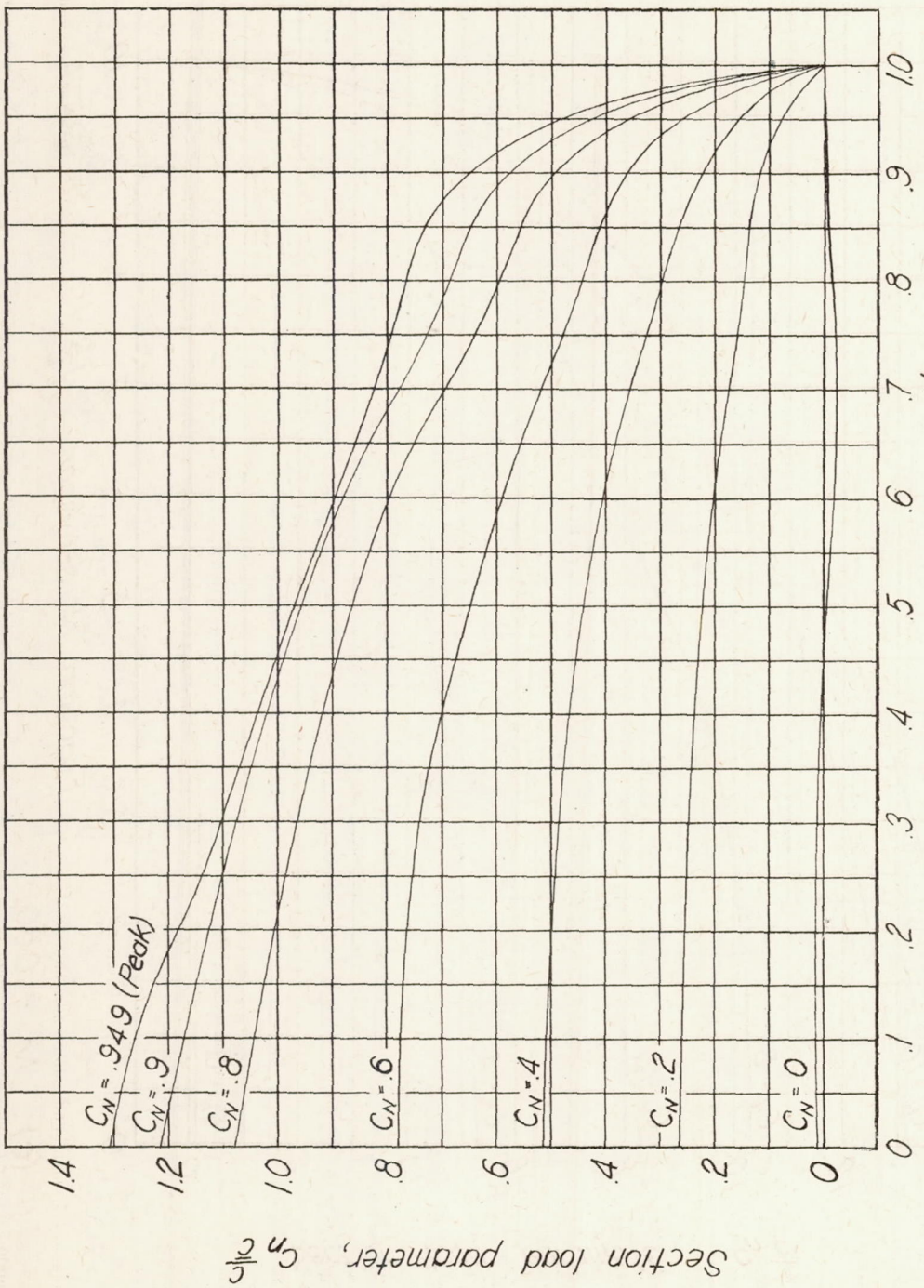

(b) $M_o = 0.40$.

Figure 15.- Continued.

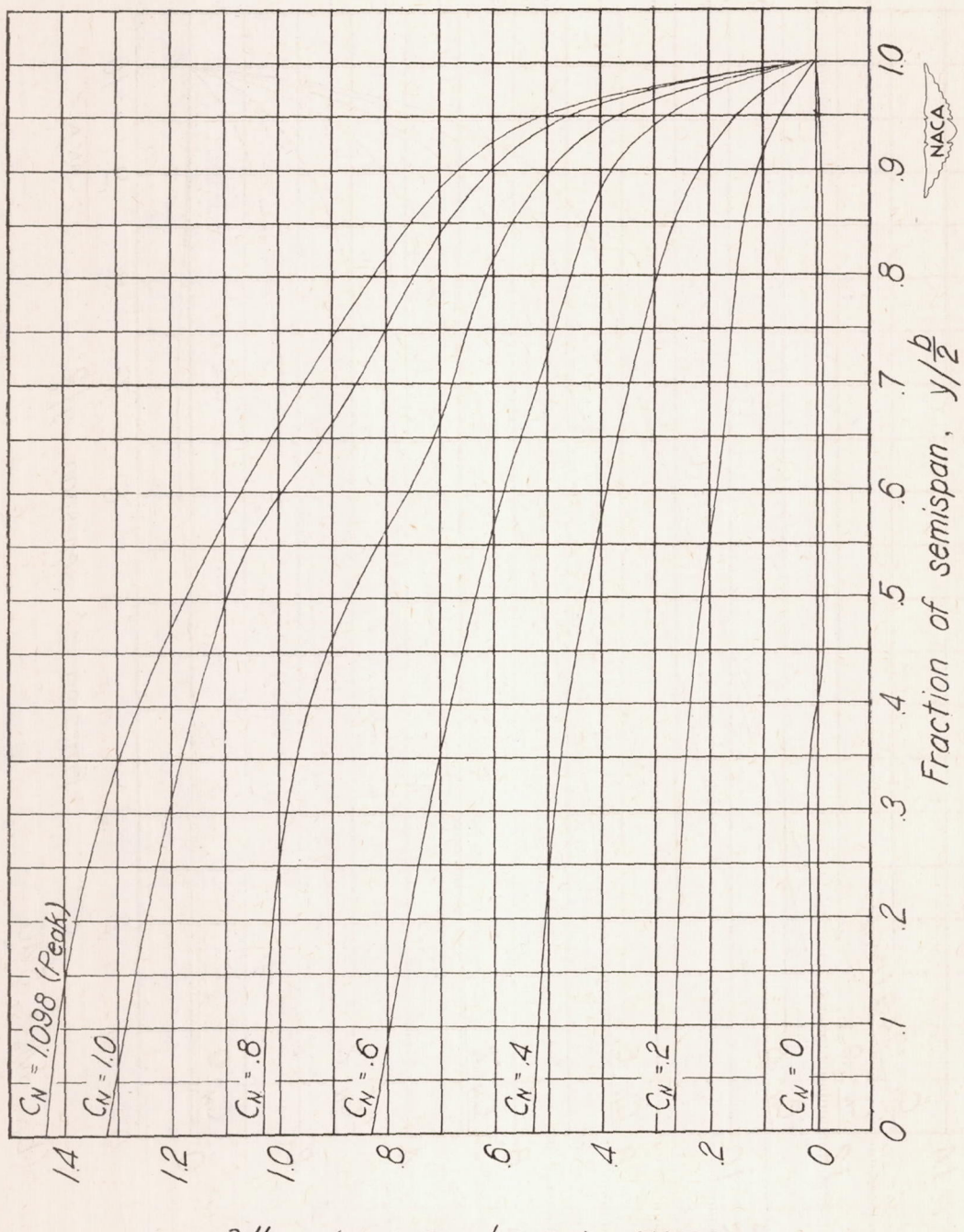

(c) $M_o = 0.60$.

Figure 15.- Concluded.

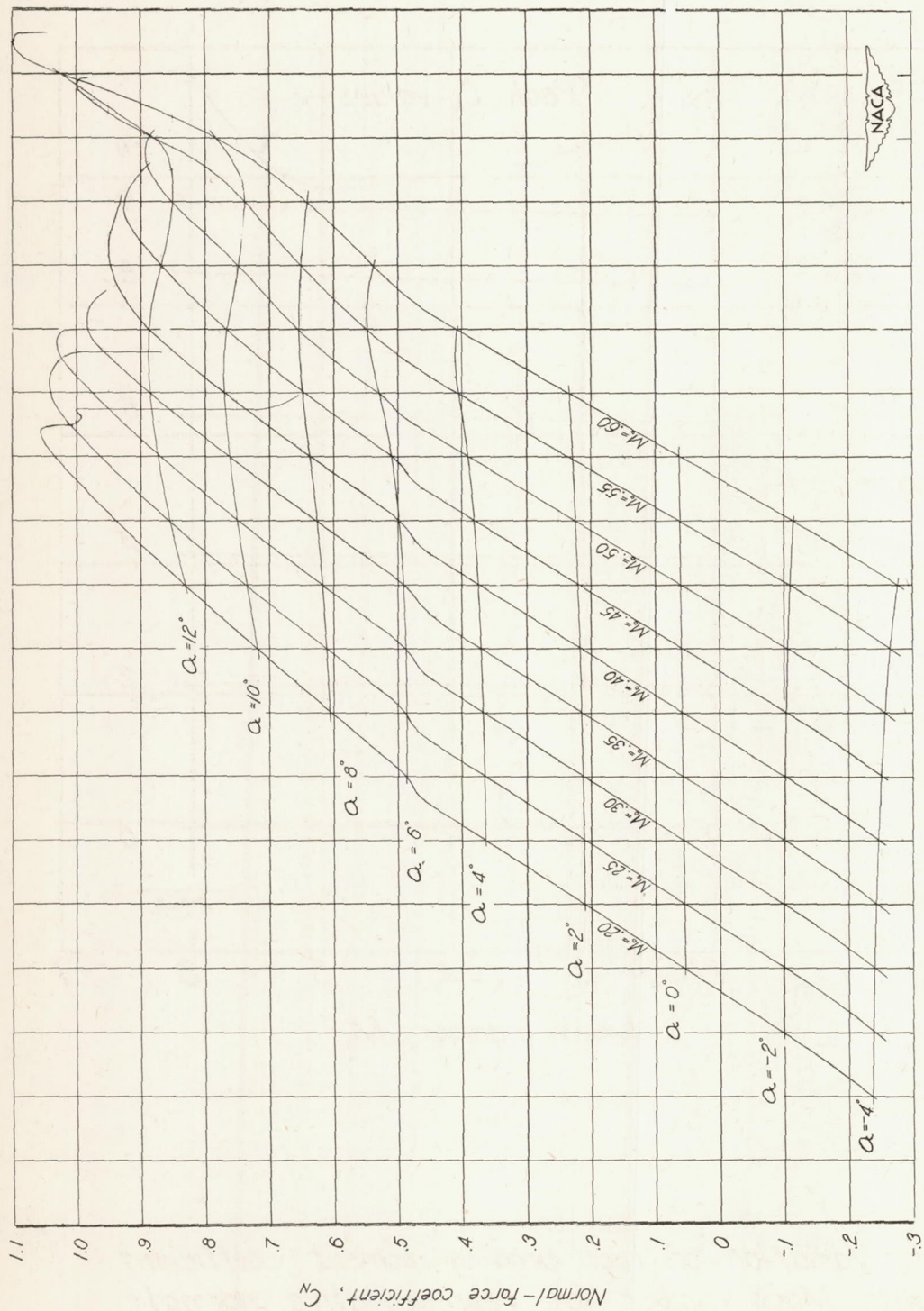

Figure 16.- Wing normal-force coefficient as a function of angle of attack and Mach number.

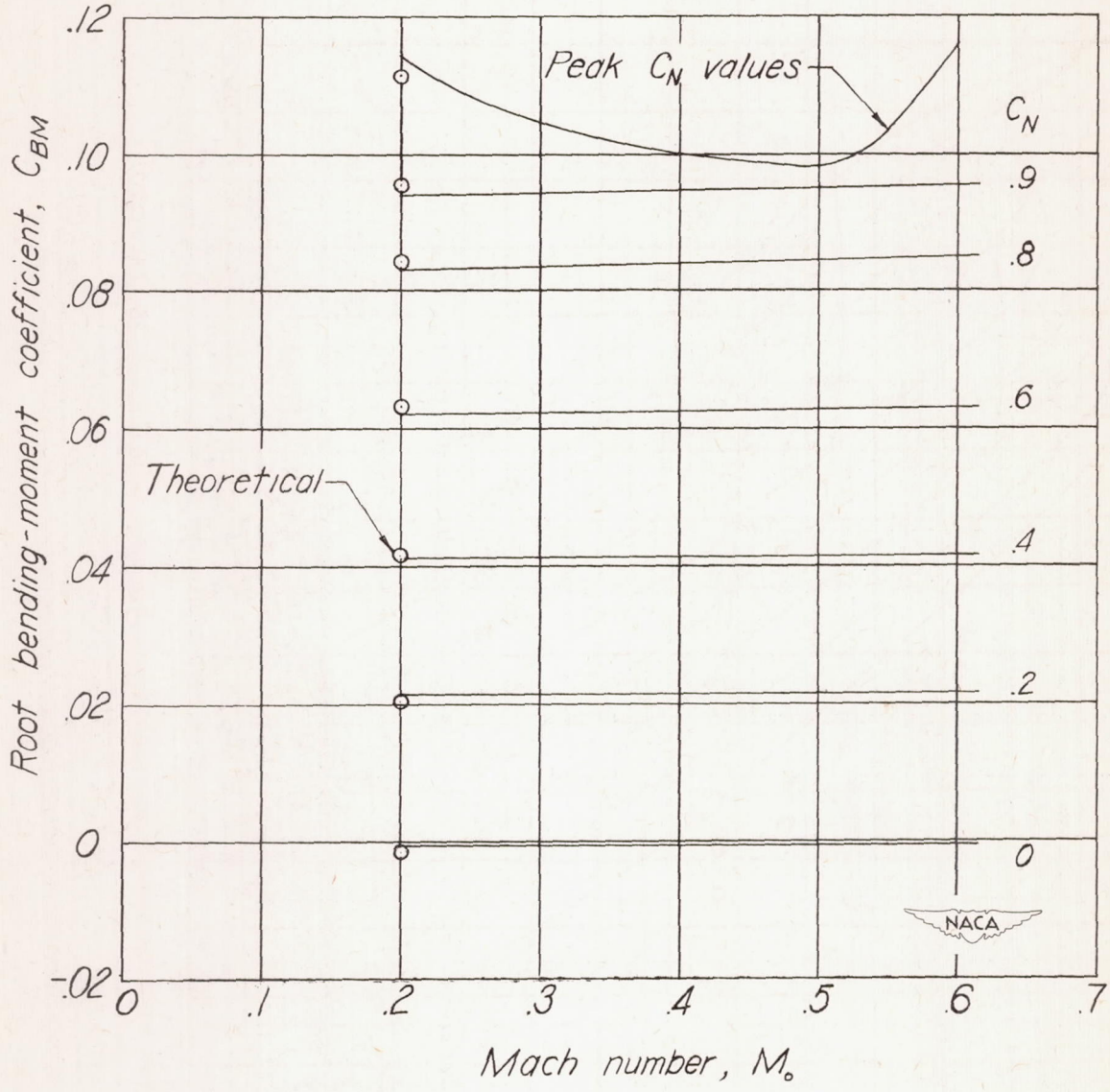

Figure 17.- Variation of root bending-moment coefficient with Mach number for representative normal-force coefficients.

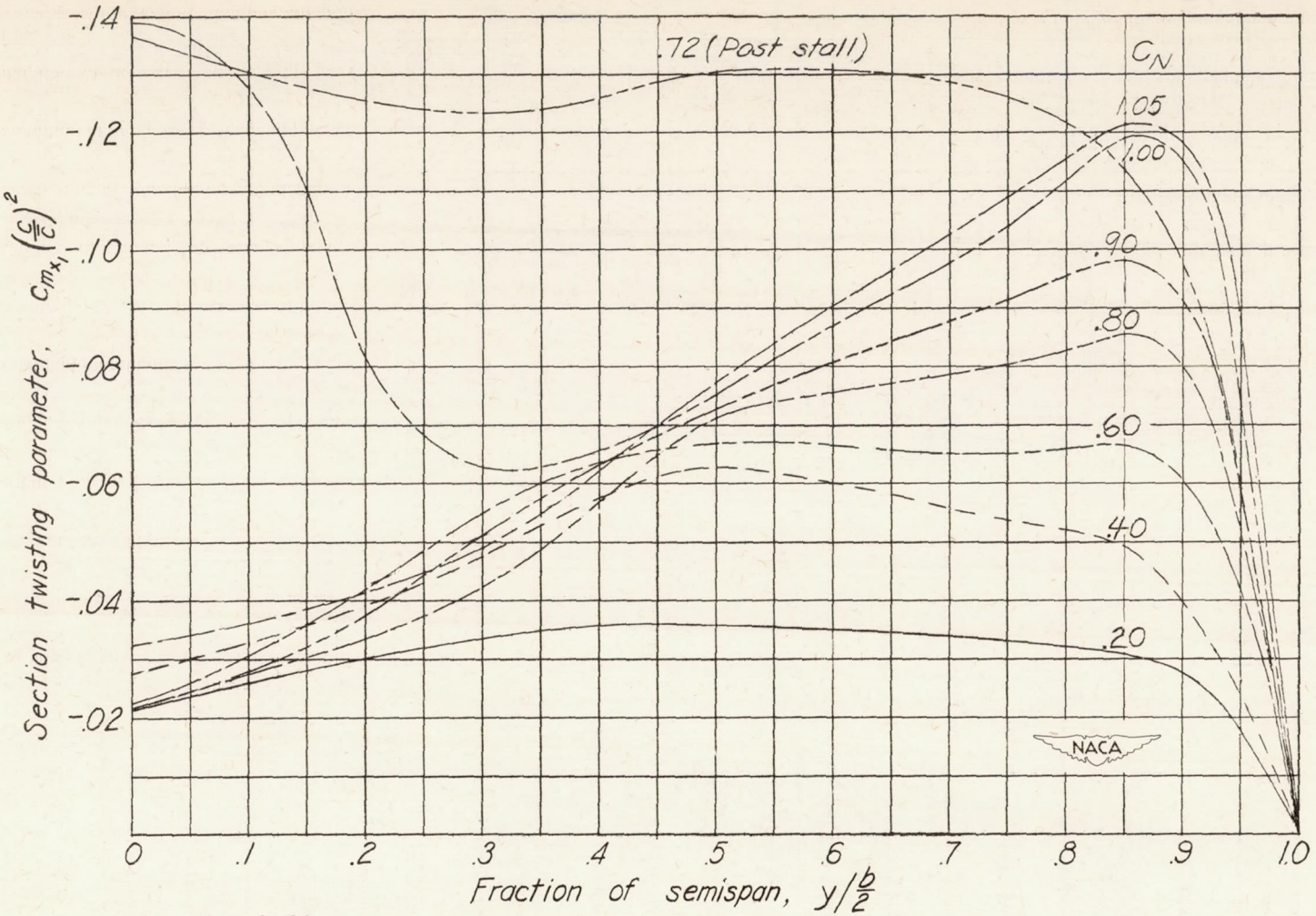

(a) $M_o = 0.20$.

Figure 18.- Spanwise variation of section twisting-moment parameter with normal-force coefficient for Mach numbers of 0.20, 0.40, and 0.60.

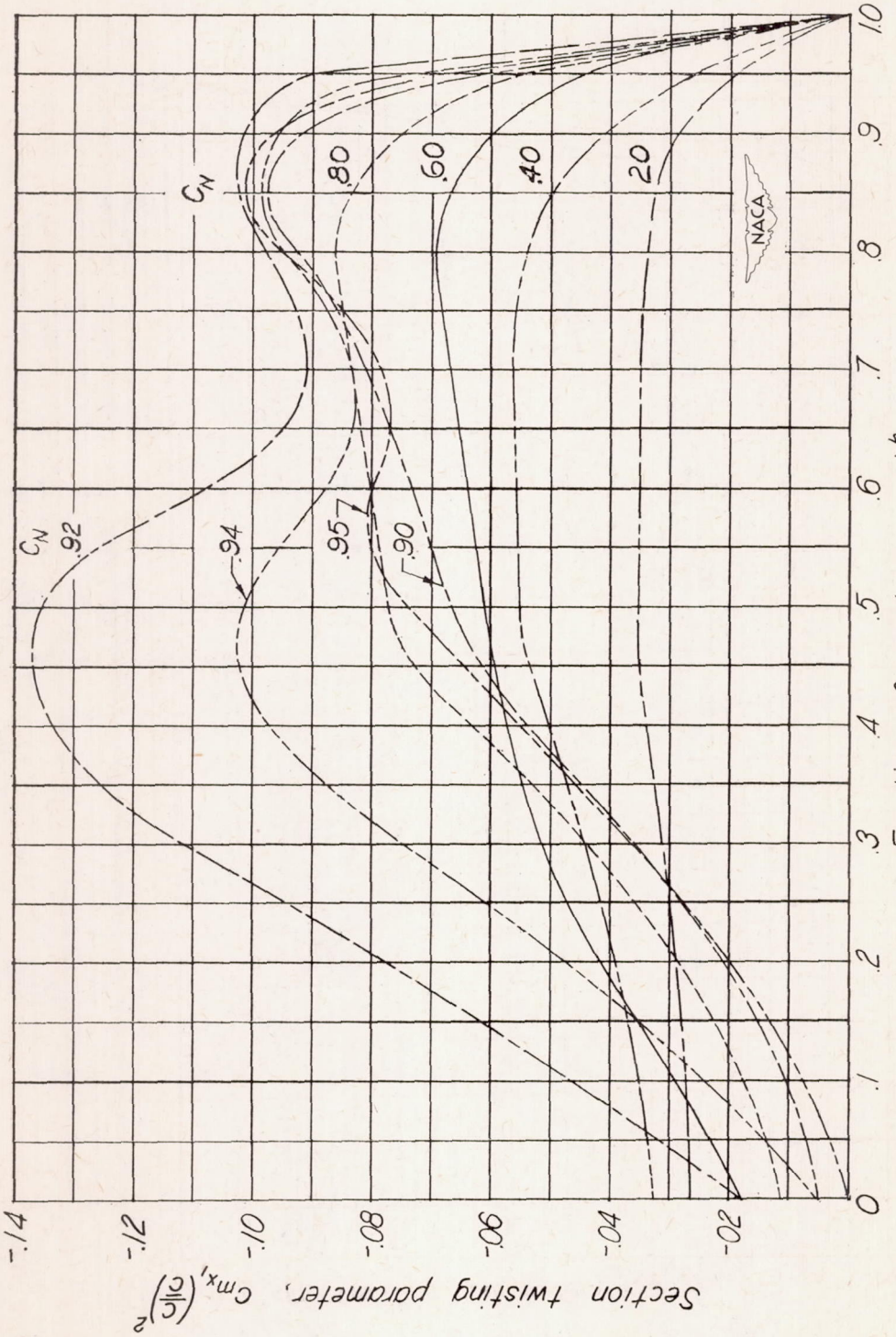

(b) $M_o = 0.40$.

Figure 18. - Continued.

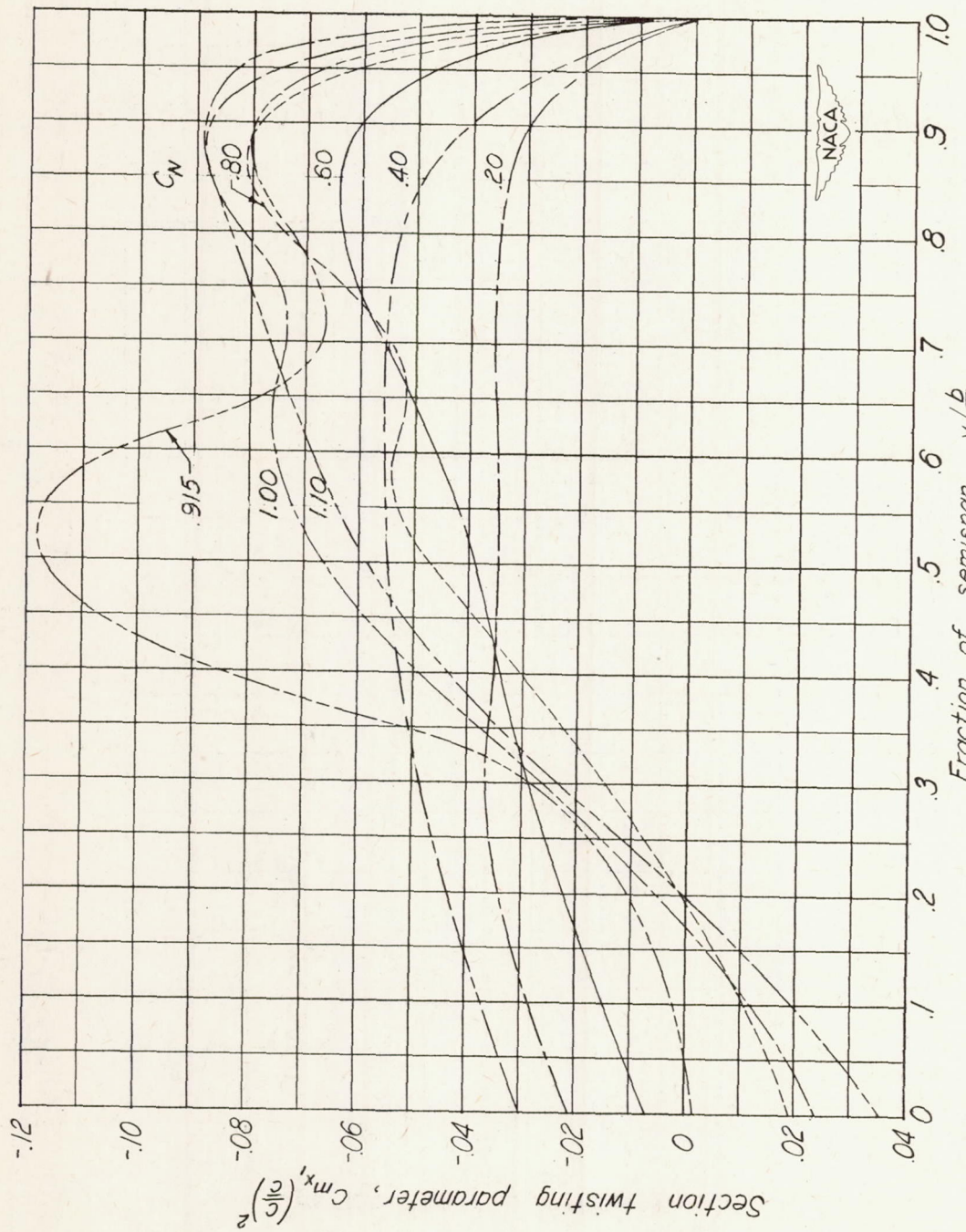

(c) $M_0 = 0.60$.

Figure 18.- Concluded.

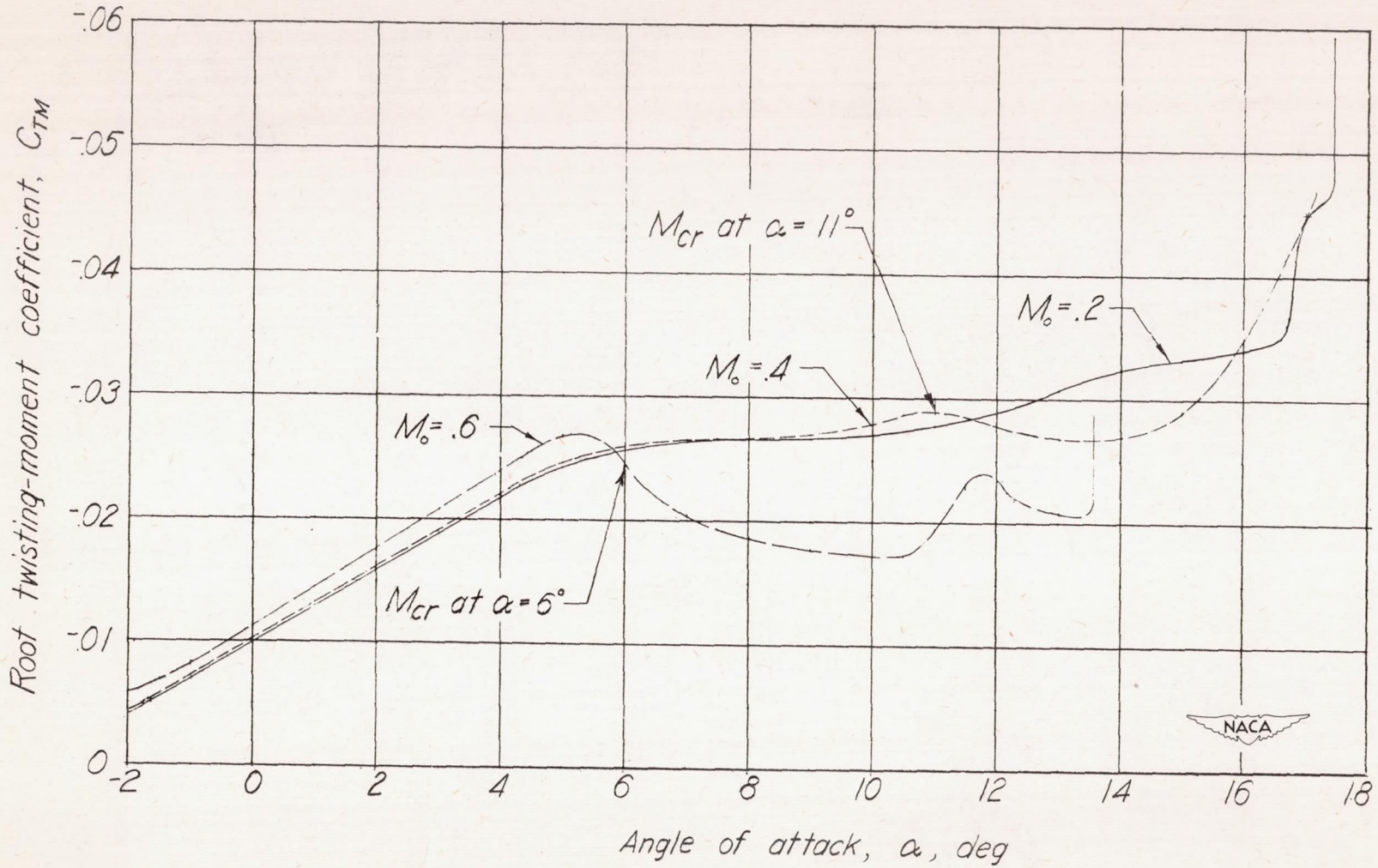

Figure 19.- Variation of root twisting-moment coefficient with angle of attack for Mach numbers of 0.20, 0.40, and 0.60.